Primate pre-arcuate cortex actively maintains persistent representations of saccades from plans to outcomes

Ioana Calangiu[1†], Sepp Kollmorgen[1], John Reppas[2] and Valerio Mante[1†]

1. Institute of Neuroinformatics and Neuroscience Center Zurich
University of Zurich and ETH Zurich, Switzerland.

2. Department of Neurobiology and Howard Hughes Medical Institute
Stanford University, USA.

† Corresponding Authors: **calangiu@ini.uzh.ch**, **valerio@ini.uzh.ch**

Abstract

Dorso-lateral prefrontal cortex is thought to contribute to adaptive behavior by integrating temporally dispersed, behaviorally-relevant factors. Past work has revealed a variety of neural representations preceding actions, which are involved in internal processes like planning, working memory and covert attention. Task-related activity following actions has often been reported, but so far lacks a clear interpretation. We leveraged modified versions of classic oculomotor paradigms and population recordings to show that post-saccadic activity is a dominant signal in dorso-lateral prefrontal cortex that is distinct from pre-saccadic activity. Unlike pre-saccadic activity, post-saccadic activity occurs after each saccade, although its strength and duration are modulated by task context and expected rewards. In contrast to representations preceding actions, which appear to be mixed randomly across neurons, post-saccadic activity results in representations that are highly structured at the single-neuron and population level. Overall, the properties of post-saccadic activity are consistent with those of an action memory, an internal process with a possible role in learning and updating spatial representations.

Introduction

Goal-directed behavior often requires animals to perform coordinated sequences of multiple different actions. Individual actions within a sequence are selected based on a variety of behaviorally relevant factors, often distributed in time, such as past and present perceptual inputs, previous actions, plans of future actions, and the environment's reward structure. In primates, the ability to form, maintain and combine representations of these factors is thought to depend on a network of hierarchically organized brain areas that extends from the premotor cortex to the anterior PFC, whereby areas along the hierarchy process progressively more abstract and temporally dispersed signals[1–3].

Within this processing hierarchy, the dorso-lateral prefrontal cortex (dlPFC) is thought to play a key role for behaviors requiring flexible action selection. For instance, imaging studies revealed that sequential behaviors recruit dlPFC only at the beginning of the learning phase[4–6] or when they contain flexible stimulus-action associations[7–9], while rigid, overlearned behavioral sequences do not typically engage the dlPFC, however complex they might be[10–

[12]. In agreement with these findings, humans with dlPFC lesions[13–15] can perform individual actions but show difficulty in organizing these actions into action sequences[16,17].

Electrophysiological recordings in the dlPFC of monkeys engaged in behavioral tasks have revealed representations of task-dependent variables that are involved in learning and executing flexible, goal-directed behaviors[18–21]. Many of the identified representations are thought to contribute to processes leading to an upcoming decision. This includes short-lived, working memory traces of stimulus features like spatial location[22,23], color[23], image[24] or sound identity[7], as well as the maintenance and deployment of attention[25], the accumulation of relevant sensory evidence[26,27], planning of future actions[28], and the representation of expected outcomes[29,30] and values[31]. Such representations have been the focus of influential modeling efforts aimed at uncovering the computational principles underlying decision-formation in dlPFC networks[32–36] and overall have significantly shaped the current understanding of dlPFC functions and its prominent contributions to decision-making[18,37–39].

Beyond representing factors immediately relevant for the selection of future actions, dlPFC neurons are also modulated by features related to past actions, like experienced rewards[40] or past choices[41]. Representations of such factors or task variables can persist in dlPFC across several trials of a task[40,42,43]. One prominent, widely reported signal that appears to be linked to past actions is post-saccadic activity, which in several areas of dlPFC is intermingled with pre-saccadic and movement related activity[9,28,44,45]. The prevalence of post-saccadic activity suggests that it may play a key role in the function of dlPFC[46]. The possible computational role of post-saccadic activity, however, has largely remained elusive, mostly because past studies have resulted in somewhat contradictory findings about its properties.

Here we studied post-saccadic activity in pre-arcuate cortex of primates engaged in novel variants of classic oculomotor tasks. Several new features of our experimental design allowed a more precise and conclusive characterization of the properties of post-saccadic activity than previously possible. Surprisingly, we found that saccade-related activity in pre-arcuate cortex was consistently strongest not before or during saccades, but rather following each saccade. The properties of post-saccadic activity are consistent with those of an *action-memory*, a sustained representation of the previously performed action[47]. Such action-memories are represented in dlPFC after every saccade, and induce largely stereotypical neural dynamics following the planning and execution of a saccade, suggesting a tight, structured relation between the representations of future and past actions in dlPFC.

Results

Behavioral task and neural recordings

Three monkeys were engaged in a visually-guided, delayed-saccade task, requiring them to perform a sequence of saccades and fixations on each trial to obtain a reward (Figure 1a). A trial was initiated by a saccade to the fixation point. Subjects were required to maintain fixation until disappearance of the fixation point (1.3-2.1s after trial initiation). At 0.6-0.8s after the onset of the fixation point, a saccade target was presented in the periphery (33 unique positions per experiment). Monkeys were then required to execute the saccade to the target when the fixation point disappeared after an interval of random duration following the target onset (0.7-1.3s). After the saccade, monkeys were again required to maintain fixation,

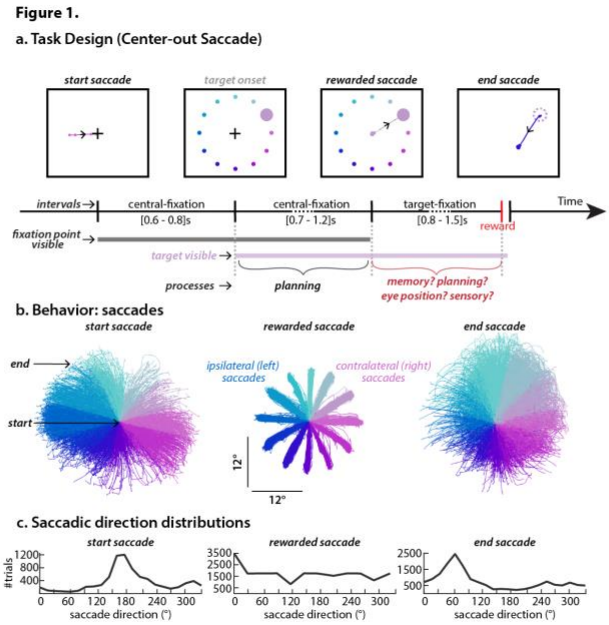

Figure 1. ***Behavioral task and neural responses in PFC. a.*** *Monkeys performed a visually-guided, delayed-saccade task. After a monkey initiated fixation, a single visual target (large circle) appeared on the screen at one of 33 possible locations (small circles, only 12 shown). After a delay of random duration, the fixation-point (cross) disappeared, cuing the monkey to rapidly execute a saccade towards the target. The monkey then had to fixate on the target for a period of random duration that ended with the delivery of reward.* ***b.*** *Top: Eye-trajectories for three types of saccades: start saccades towards the fixation-point, which initiate the trial; rewarded saccades, towards the visual target; and end saccades; away from the fixation point. Eye trajectories are sorted by saccade direction. The starting location was subtracted from the eye-trajectories of the start and end saccades, meaning that all saccades start from the center of the respective "point clouds". The direction of start and end saccades are discretized into classes that match the fixed directions of the rewarded-saccade in the corresponding session.* ***c.*** *Distribution of saccade-direction for the three different saccade types pooled over all sessions. Saccades from the target back to the fixation point are included in the end-saccades, not in the start-saccades, resulting in fewer start than end saccades. We only included start and end saccades with amplitudes similar to those of the rewarded saccade (4-16 deg).*

this time on the target, for the duration of a final random time interval (the delay period, 0.8-1.5s). At the end of this interval, the target disappeared, a reward was delivered, and there were no task constraints on the subjects' eye movements.

We analyzed neural activity and eye movements for all trial epochs (Figure 1a) and different types of saccades, i.e. the instructed and freely initiated saccades occurring before, during, and after each trial (Figure 1b). We refer to the initial saccade to the fixation point as the "*start saccade"*, the saccade to the target as the "*rewarded saccade"*, and the first saccade away from the target after reward delivery as the "*end saccade".* Figure 1c shows the saccade-direction distribution for the different saccade types pooled over all experiments. On some trials, the end saccade leads back to the fixation point and thus corresponds to the start saccade, hence there are fewer start saccades than end saccades. Moreover, we only include start and end saccades with amplitudes similar to the experimentally-set amplitudes of the rewarded saccade, i.e. between 4 and 16 deg. The start saccade is followed by the "*central-fixation",* i.e. the initial fixation on the fixation point lasting for a randomized interval (1.3-2.1s) and preceding the "*rewarded saccade*". The *rewarded saccade* is followed by the "*target-fixation*" lasting for a randomized interval (delay period, 0.8-1.5s), i.e. the fixation on

the target until it disappears (Suppl. Fig. 1b). The inclusion of this *target-fixation* delay period is a key difference with instructed-saccade tasks used in past studies[28,48–51] and greatly simplifies the interpretation of post-saccadic neural activity.

Neural activity was recorded with 96-channel Utah-arrays implanted in pre-arcuate cortex, a region of dorso-lateral PFC close to, and possibly including, the most rostral part of the frontal eye fields[52] (Supp. Fig. 1a). The data presented were collected when the monkeys were proficient in performing the task: there are no error trials and the direction of the rewarded saccade always refers to the target location. Below, we focus on the results from monkey T (20,952 trials from 9 experiments, 1706 single and multi-units). The analogous results from monkeys V and C are presented in supplementary figures (4751 and 8611 trials, 10 and 10 experiments, 2334 and 2095 units).

Post-saccadic activity in prefrontal units

We begin our analysis by considering neural activity at the level of individual units, aligned to the onset of the *rewarded saccade*. In agreement with a large body of past literature[28,48–51,53], the activity of many units is modulated by saccade direction before the saccade (Figure 2a, top row) and/or *during* saccade execution (Figure 2a, middle row) . However, directional selectivity often does not disappear after the saccade is concluded—in many units, activity is strongly modulated by saccade direction also (or only) at times *following* the saccade (Figure 2a, e.g. bottom row).

The *preferred direction* of a given unit, defined as the saccade direction eliciting the largest activity, appears to be largely constant over time for some units (e.g. Figure 2a, unit 7), while it shows prominent changes between pre-saccadic and post-saccadic times in other units (Figure 2a, unit 3).

To quantify the strength of directional selectivity in single units at any given time, we fit a simple descriptive model to a unit's activity averaged by target direction[28]. Even though target location varied both with respect to direction and distance from the fixation point (not shown in Figure 1a), the model includes bell-shaped tuning only for direction, as eccentricity values were not varied over a sufficiently large interval. The two main model parameters determining the directional selectivity are *response gain*, which determines tuning strength, and *preferred direction*.

These fits show that directional selectivity, surprisingly, is most pronounced at times following the saccade. In Figure 2b, we consider response gain and goodness of fit around the time of the rewarded saccade. Directional selectivity is strongest (i.e. large response gain and goodness of fit) in the early post-saccadic window, when the saccade is already concluded and the eye is stationary (duration of rewarded saccade = 40±10ms; data for other monkeys in Supp. Fig. 3a, f). Note that this pronounced directional selectivity does not seem to be related to the visual selectivity at target onset, a first indication that it is movement, not sensory related (Suppl. Fig. 2). Remarkably, long after the end of the saccade, the strength of selectivity and the level of activity across the population are still comparable to that observed immediately before saccade onset. Selectivity plateaus at a high level about 800ms after the saccade has ended. A similar plateau is reflected in the mean population response (last row in Figure 2a; Suppl. Fig. 3a, f other monkeys).

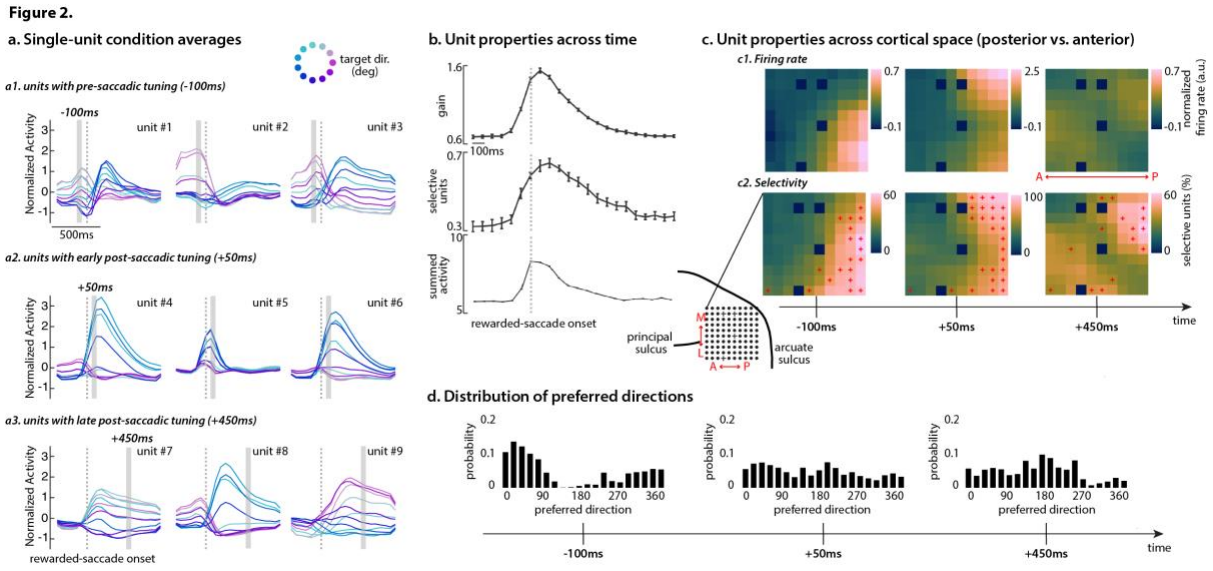

Figure 2. ***Single-unit representation of the rewarded saccade****.* ***a.*** *Condition-averaged responses of individual units. Example responses for units with high goodness-of-fit* ***before*** *(a1),* ***immediately after*** *(a2) and* ***long after*** *the saccade (a3) are averaged and colored according to the direction of the rewarded-saccade.* ***b.*** *Condition-averaged responses are fit by a simple, time-dependent descriptive model. One model parameter, gain, quantifies the strength of tuning (upper row). A unit is considered selective (middle row) if the cross-validated goodness-of-fit measure (r-squared) is larger than 0 (i.e. direction tuning is better described by the model than by a constant firing rate). Raw summed activity of the entire population is also stronger after the saccade (bottom row). Error bars represent s.e.m. across the 9 sessions.* ***c.*** *Firing rate and selectivity computed at each electrode location (96 locations). Dark blue squares mark the four ground electrodes. c1. Mean firing rate of condition averaged responses, z-scored across time. c2. Mean percentage of selective units. Red crosses indicate values outside the 95% confidence intervals of a shuffled null-distribution assuming no relation between unit selectivity and electrode location. The color scale is identical for the pre-saccadic (-100ms) and late post-saccadic (+450ms) properties to facilitate a direct comparison between these times. Early post-saccadic (+50ms) properties are shown with a different color scale, due to the elevated values at that time.* ***d.*** *Preferred direction of all selective units from all recording sessions, at three times relative to rewarded-saccade onset. Preferred direction is one of the model's parameters and reflects the saccade direction that elicits the highest response at the corresponding time.*

The prevalence of directional selectivity across recording locations in pre-arcuate cortex (Figure 2c), as well as the corresponding preferred directions (Figure 2d, Suppl. Fig. 2a), differ between pre and post-saccadic activity. Pre-saccadic selectivity, which reflects the direction of the upcoming saccade, is most common at posterior locations, close to the expected location of the frontal eye fields (Figure 2c, top row (c1) mean firing rate and bottom row (c2) selectivity, time = -100ms). At these locations, pre-saccadic tuning is strongly biased towards contralateral target directions, as expected from previous studies[7,9,28,52] (Figure 2d, time = -100ms). Post-saccadic selectivity, which reflects the direction of the preceding saccade, is more evenly distributed across recording locations, although the most pronounced early and late selectivity are observed at different locations. The strongest early post-saccadic activity occurs at posterior locations (Figure 2c, time = +50ms) but then spreads to anterior locations (Figure 2c, time = +450ms; Suppl. Fig. 3b, g other monkeys). The preferred saccade direction for late post-saccadic activity, in particular, is more evenly distributed between contralateral and ipsilateral directions than for pre-saccadic activity (Figure 2d; Suppl. Fig. 3c, h, other three monkeys). These differences in cortical spatial arrangement and functional organization are

154 further indications that pre- and post-saccadic activity may represent distinct kinds of signals.
155 This conclusion is corroborated by the analyses presented below.

156 ## Sustained encoding of saccade direction at the population level

157 Given the existence of prominent pre- and post-saccadic directional selectivity in individual
158 units, we expect that the direction of the rewarded saccade is reliably represented also in
159 single-trial population activity. We quantify the representation of saccade direction in single-
160 trial population spike-counts using cross-validated multi-class decoders[54–57] (Figure 3; Suppl.
161 Fig. 6b, h other monkeys; Suppl. Fig. 4 for other decoders). We first trained decoders that
162 decode saccade direction from population spike counts at particular times relative to the
163 saccade onset. Post-testing, we sort the results according to the true saccade laterality on
164 each trial (contralateral and ipsilateral target directions) to emphasize the differences in
165 hemifield representations (Figure 3a, see legend).

166 Cross validated decoding accuracy varies over time and across saccade directions, echoing
167 the prevalence and properties of tuning in individual units discussed above (i.e. Figure 2). For
168 all target directions, decoding accuracy peaks after the end of the saccade, but persists
169 throughout the target-fixation, and is still high at and after reward delivery (up to 1.5s after
170 saccade onset; Figure 3a, right; Suppl. Fig. 6b, h other monkeys). Throughout the *central-*
171 *fixation* period, the execution of the rewarded-saccade, and the *target-fixation* period,
172 decoding errors almost exclusively reflect read-out directions that are immediately adjacent
173 to the true direction (Figure 3c, top row, Time-specific read-out), reflecting the smooth tuning
174 for direction in individual units (Figure 1c). Decoding accuracy remains high well beyond the
175 time of the saccade than could be accounted for by transient inputs from motor or sensory
176 areas. Like pre-saccadic activity, post-saccadic activity may thus be a form of persistent,
177 internally generated activity[9,51].

178 Further insights into the dynamics of saccade representations can be obtained by comparing
179 the properties of decoders trained at different times[33,58–62]. Specifically, we applied the
180 decoders trained at any given time in the trial on activity recorded at a different time, and
181 then analyzed both the accuracy of the read-out (Figure 3b; Suppl. Fig. 6e, k other monkeys)
182 and the statistics of the errors (Figure 3c). This analysis indicates that late pre-saccadic
183 representation of saccade direction is static, as a decoder trained at one pre-saccadic time
184 works well at all other pre-saccadic times (Figure 3b; Suppl. Fig. 6e, k other monkeys; bottom-
185 left). The post-saccadic representation instead is highly dynamic early after saccade offset,
186 and may remain dynamic even late in the target-fixation, as any particular post-saccadic
187 decoder does work best at the time it was trained (large diagonal values in middle part, Figure
188 3b; top-right in Suppl. Fig. 6e, k other monkeys).

189 The representation of saccade direction across the population differs strongly between pre
190 and post-saccadic times[63,64]. Decoders trained during the *central-fixation* lead to poor
191 decoding performance during the *target-fixation* (Figure 3b; bottom-right), and vice versa
192 (Figure 3b; top-left). However, the resulting pattern of read-out errors indicates that the
193 relation between pre- and post-saccadic representations is not random: for pre-saccadic
194 decoders applied to post-saccadic activity, the read-out is strongly biased towards the
195 direction *opposite* to the true saccade direction (Figure 3c, pre-saccadic decoder; decoding
196 error = 180°). The bias is strongest shortly after completion of the rewarded saccade, but

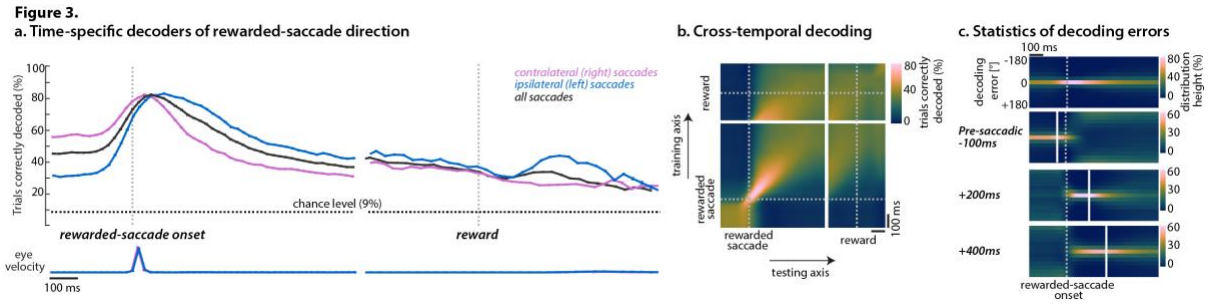

Figure 3. ***Population-level representation of the rewarded-saccade****.* ***a.*** *Time-specific decoding of the direction of the rewarded saccade. At each time relative to the rewarded saccade (horizontal axis), a separate multi-class decoder (linear discriminant analysis) is trained to predict the direction of the rewarded saccade based on the population response. The vertical axis shows 10-fold cross-validated decoding performance. Decoders are trained and tested on 11 classes (all directions of rewarded-saccades during one session) meaning that chance performance is 9%. Post-testing, the decoding results are grouped based on the laterality of the rewarded-saccade (contralateral and ipsilateral). The lower panel displays the eye velocity averaged within each category, showing stable fixation prior and post saccade execution.* ***b.*** *Cross-temporal decoding, showing how well a particular time-specific decoder generalizes to other times. The vertical axis shows the time at which the decoder was trained, the horizontal axis the times at which it was tested (times relative to onset of the rewarded saccade or reward delivery). Color indicates test performance. The diagonal (bottom-left to top-right) corresponds to the black curve in a.* ***c.*** *Time-dependence of decoding errors; the distribution of angular errors (vertical axis) when testing times (horizontal axis) are chosen to coincide with training times (time-specific decoders; top) or when testing times are different than training times (cross-temporal decoders; bottom three plots). Training times of cross-temporal decoders are -50ms, +200ms, +400ms relative to the rewarded-saccade onset (solid lines).*

persists throughout even the longest target-fixations (Suppl. Fig. 5). A similar, but weaker, effect occurs when post-saccadic decoders are applied to pre-saccadic activity (Figure 3c; post-saccadic decoders defined at +200 and +400ms). This "flip" of population representations leads to an overall performance that is lower than chance level (Figure 3b, top-left and bottom right corners), and mirrors the flip in preferred direction observed in the tuning of some individual units (Figure 1c; e.g. units 1 and 3).

Interpreting this flip observed in saccade representation is not trivial, because monkeys often direct the first saccade after the rewarded saccade (end-saccade) back towards the center of the screen (Figure 5b, middle matrix). If monkeys started planning the end-saccade already during the target-fixation, the resulting preparatory activity would tend to be strongest in units with preferred directions opposite that of the rewarded saccade, thus potentially explaining the observed flip in representations[28]. Similar behavioral regularities are common in instructed saccade or reach tasks[65], and indeed have led previous studies to conclude that the prominent post-movement activity they observed may be the preparatory activity for the next movement the animal will produce[28]. Below we show that, for post-saccadic activity in pre-arcuate cortex, this conclusion is incorrect.

Post-saccadic activity is not preparatory activity for the next saccade

Post-saccadic activity does not encode the direction of the next saccade because: (1) many units with significant post-saccadic tuning do not display pre-saccadic tuning; (2) the dynamics of single unit selectivity, together with the flip in decoding, does not depend on the next saccade; and (3) if behavioral regularities between the rewarded and end saccade are

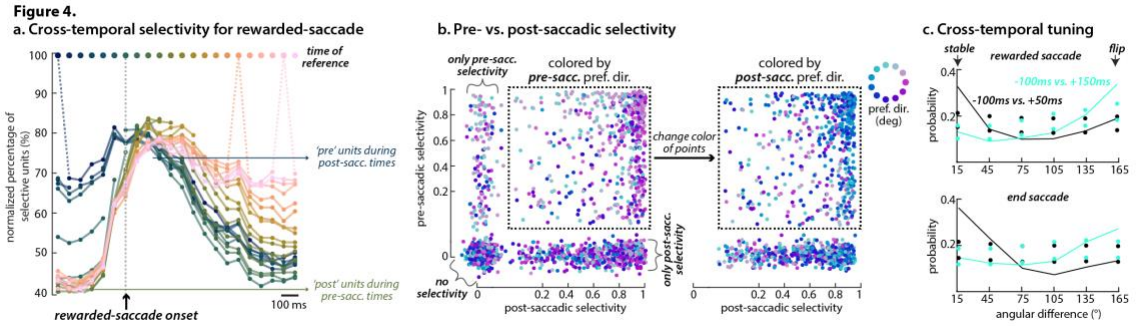

Figure 4. ***Dynamics of directional selectivity in single units***. ***a.*** *Cross-temporal selectivity for the rewarded saccade. Colored curves show the percentage of units that are selective both at a reference time (color indicates reference time, circles on top) and at other times in the trial (horizontal axis). For each curve, the lines connecting the corresponding reference time and the two immediately adjacent times (dashed) are mostly omitted. Units selective at a reference time preceding the saccade are more likely to be selective at other pre-saccadic compared to post-saccadic times (green colors), while units selective at reference times following the saccade are more likely to be selective at other post-saccadic compared to pre-saccadic times (pink colors).* ***b.*** *Pre-saccadic (-100ms, vertical axis) vs. post-saccadic selectivity (+150ms, horizontal axis), quantified as the goodness-of-fit of the direction-tuning model at these times. Each point represents a unit. Color is the preferred direction before (left panel) and after (right panel) the saccade. Some units only have pre-saccadic tuning (close to the vertical axis), more units only have post-saccadic tuning (close to the horizontal axis) and many have both (rectangle). The latter change their tuning from predominantly contralateral (rightward, purple) to predominantly ipsilateral (leftward, blue).* ***c.*** *Cross-temporal tuning. Each plot shows a histogram of angular difference between the pre-saccadic and post-saccadic preferred directions over all units that are selective at both times (curves; points: 5th and 95th confidence intervals of a shuffle null-hypothesis assuming no relation between pre- and post-saccadic preferred directions). Bins of 30 degrees length are centered along the horizontal axis. At +50ms, the post-saccadic and pre-saccadic preferred directions tend to match (peak of distribution at 15° - [0: 30] degrees, "stable"), but at +150ms the preferred directions has mostly flipped (peak of distribution at 165° - [150: 180] degrees, "flip") for both the rewarded (top) and end saccade (bottom).*

accounted for, the direction of the end-saccade cannot be predicted from the activity during the *target-fixation.* Below we detail the analyses behind these three statements.

First, among all units with significant post-saccadic tuning, about half do *not* display pre-saccadic tuning (Figure 4b, points close to the horizontal axis where pre-saccadic selectivity is 0; Suppl. Fig. 3d, i other monkeys). In that half of the population, post-saccadic activity thus cannot be the pre-saccadic activity for the upcoming saccade. To compare the strength of tuning in individual units across time, we define a "cross-temporal selectivity" measure (Figure 4a), which quantifies the percentage of units that are tuned for saccade direction both at a given reference time (small circles on top and curve of the corresponding color) as well as at a different comparison time (horizontal axis). The highest values of cross-temporal selectivity are observed within the pre- and post-saccadic epochs meaning that many units have sustained pre-saccadic tuning, but no post-saccadic tuning, or sustained post-saccadic tuning, but no pre-saccadic tuning (Figure 4a, lines with dark colors at times before the saccade and lines with light colors at times after the saccade). A comparison of the directional selectivity at a pre-saccadic time and a post-saccadic time shows an interesting asymmetry: a comparatively large fraction of units with pre-saccadic tuning also displays post-saccadic tuning (Figure 4a, dark blue horizontal arrow), but only a smaller fraction of units with post-saccadic tuning also displays pre-saccadic tuning (Figure 4a, green horizontal arrow).

Second, the dynamics of single unit selectivity is linked to the saccade the monkey is performing, not the future saccade. In units that show both pre- and post-saccadic tuning, the relation between pre and post-saccadic activity is not random: their preferred hemifield tends to flip, from contralateral to ipsilateral (Figure 4b, predominant color of points is purple and blue at -100ms and +150ms, respectively). The flip in preferred hemifield is however not immediate, since at +50ms, right after movement completion, the pre-saccadic preferred hemifield is preserved (upper row in Figure 4c; Suppl. Fig. 3e, j other monkeys). This dynamics in selectivity of individual units matches the flip in decoding observed at the level of the population (Figure 3c). Analogous dynamics in selectivity occurs for end saccades (lower row in Figure 4c) suggesting that prefrontal networks undergo a stereotypical reconfiguration around every saccadic event.

Consistent with the observation at the level of single units, we find that saccade direction can be robustly read out from the population also after the start and end saccades (Figure 5a, duration of start saccade = 30+-30ms; duration of end saccade = 140+-80ms; Suppl. Fig. 6d, j other monkeys). Critically, Figure 5a shows the accuracy of decoders that were trained only on activity around the *rewarded-saccade*, meaning that the same decoders have high accuracy for all three saccades and implying that the population encoding of saccadic activity is largely preserved across different types of saccades (see Suppl. Fig. 7b and c for a finer comparison at the level of error statistics and cross-temporal matrices). In particular, direction read-outs based on a pre-saccadic decoder are flipped during the post-saccadic period for both the start saccade and end saccade (Figure 5b), very much as for the rewarded saccade (Figure 3c). Crucially, the prominent regularities in the metrics of saccades that follow the rewarded saccade (Figure 5c, center; end saccades tend to be opposite to the rewarded saccade) are largely absent for the start and end saccades (Figure 5c, left and right) implying that the relation between pre and post-saccadic selectivity is not a trivial consequence of these regularities in the behavior.

Third, if the statistics of saccade directions are taken into account, the direction of the end-saccade cannot be predicted based on activity during the *target-fixation*. We used a decoder trained during the pre-saccadic epoch of the rewarded saccade (150 to 50ms before the rewarded saccade) to decode saccade direction across the *central-fixation*, the *target-fixation*, and a period after the end saccade. Notably, here the decoding procedure differs in two important ways from that in Figure 3b. For one, we use the decoder to read out the direction of the *end-saccade*, not of the *rewarded saccade*. For another, we evaluate the accuracy of the read-outs separately for trials from a single direction of the rewarded saccade. We focus on *rewarded-saccades* to the contralateral hemifield that are followed by end saccades in many different directions (Figure 5c, middle matrix). If all trials were decoded at once, the read-out flip discussed above (Figure 3c) together with the biases in the end-saccade direction (Figure 5c, middle) would trivially lead to high decoding accuracy, even in the absence of pre-saccadic activity for the end saccade. With our un-biased approach (Figure 5d), we find instead that decoding accuracy for the direction of the end-saccade is close to chance level throughout much of the central-fixation and target-fixation periods (Figure 5e; Suppl. Fig. 6c, i decoding results; Suppl. Fig. 6 a, g behavior statistics for other monkeys), in particular also at times when the read-out flip is most pronounced (Figure 3c). Accuracy increases slightly above chance level very late in the target-fixation, but to values much smaller than for decoding of the direction of the rewarded-saccade during the central-

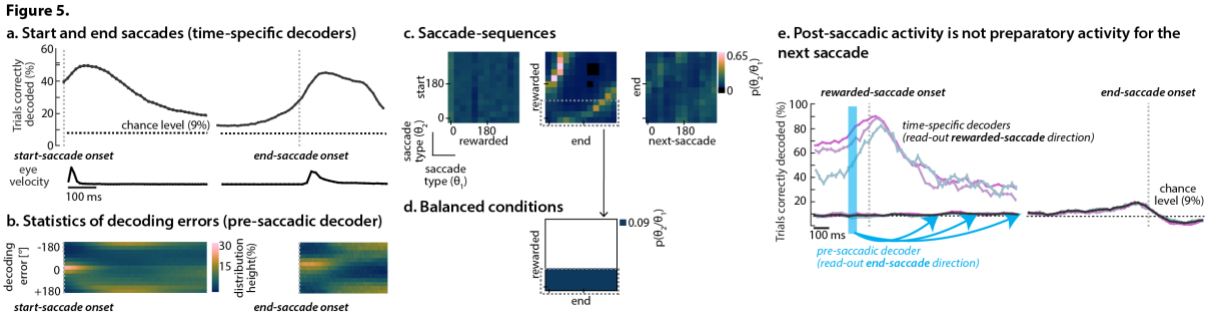

Figure 5. ***Post-saccadic activity across saccade-sequences. a.*** *Cross-validated decoding accuracy when decoding the direction of the start-saccade (left panel) and end-saccade (right panel) from responses aligned to the respective saccades. Same decoders as in Figure 3 .* ***b.*** *Angular error for the read-outs of a pre-saccadic decoder. Read-out times (horizontal axis) are aligned to those in a. The read-outs flip shortly after the saccade (error at 180 degrees).* ***c.*** *Histogram of consecutive saccades, expressed as the distribution of directions for the second saccade (columns) conditional on the direction of the first saccade (rows), shown for the start and rewarded saccade (left); rewarded and end-saccade (middle); end and the following saccade (right).* ***d.*** *Histogram of saccade-sequences of rewarded and end saccades for a balanced dataset obtained by resampling trials with rewarded saccades towards 0°, 30°, and 60°. Trials are resampled to obtain a uniform representation of end-saccade directions.* ***e.*** *Decoding the direction of the end-saccade when accounting for correlations in behavior. Bottom curves show accuracy of decoding the direction of the end saccade at various times in the trial (horizontal axis), for a decoder trained on the direction of the rewarded saccade during the corresponding pre-saccadic period (blue time-window). When the behavior correlations are eliminated (dataset in d), the direction of the end saccade cannot be predicted throughout much of the post-saccadic period (accuracy close to chance). In comparison, on the same set of trials the direction of the rewarded saccade can be decoded with high accuracy when using the time-specific decoders from Figure 3 (the three curves on top).*

fixation. Overall, the end saccade thus appears to be preceded by very little predictive activity, even at times immediately preceding saccade onset (see also Figure 5a, right).

These three observations are inconsistent with post-saccadic activity representing a plan of future action and suggest instead that post-saccadic activity is an action memory, i.e., a sustained representation of the previously performed (saccade) action.

Post-saccadic activity does not encode the momentary gaze location

The decoding analyses presented so far suggest that post-saccadic activity predominantly encodes the previous saccade in retinotopic coordinates, a representation common to all the three saccades. In principle, additional, non-retinotopic representations that differ across the three saccades could be present after each saccade, resulting in different decoding accuracies for rewarded vs. non-rewarded (start and end) saccades (compare Figure 3a and Figure 5a).

A likely candidate is a representation of the center of gaze in “head-centered” coordinates, i.e. the orientation of the eyes relative to the head[54–56,66–70]. During the target-fixation, gaze location is indistinguishable from target direction across rewarded saccades and could thus be “confounded” with the target direction in its influence on neural activity.

We directly characterized the contribution of gaze-location to post-saccadic activity in a separate behavioral task, where the saccade direction and gaze-location are somewhat decoupled and balanced (unlike for the end saccade in the instructed saccade task). Specifically, each experiment in this task included trials from two “shifted” workspaces, whereby the location of the fixation point was shifted to the left from the midline in one

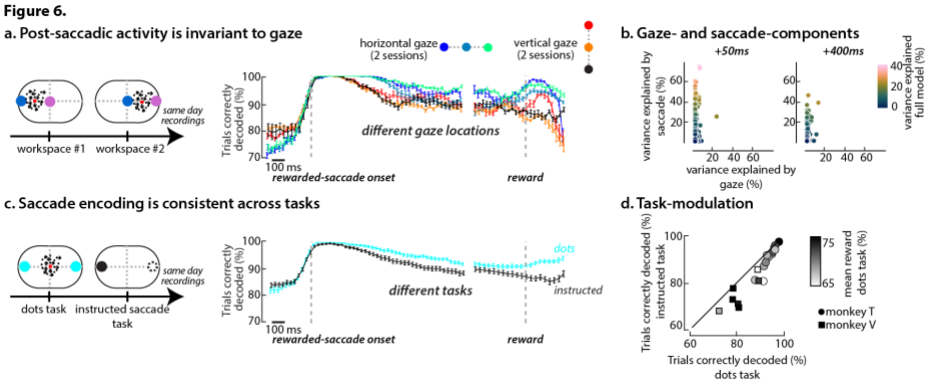

Figure 6. ***Non-retinotopic modulations of post-saccadic activity. a.*** *Decoding the direction of the rewarded-saccade across different gaze locations. Recordings from a random-dots task, where each session contained two blocks of trials that were identical but for the overall placement of the visual stimuli on the monitor ("workspaces"). We trained time-specific binary decoders on trials combined from both workspaces and evaluated accuracy with 10-fold cross-validation separately for each of the three possible target locations (displaced either horizontally or vertically; colors). The decoders achieve high accuracy across target locations.* ***b.*** *Saccade and gaze modulation at single-unit level, for the recordings in a. We modeled the activity of each unit with a regression model including linear and non-linear terms for direction and gaze. Unit activity is modulated by direction (large variance explained, vertical axis), but not gaze (horizontal axis) both early and late in the post-saccadic epoch (left and right).* ***c.*** *Decoding the direction of the rewarded-saccade across different tasks. Decoding results averaged over 11 sessions in monkey T including both the random-dots and the instructed saccade task. In both tasks, only two targets were used, placed at the same two locations. We trained time-specific binary decoders on trials combined from both tasks and evaluated accuracy with 10-fold cross-validation separately for each task (colors). The decoders achieve high accuracy across both tasks.* ***d.*** *Decoding performance at +570ms for individual sessions in monkeys T and V. Overall, post-saccadic signals are stronger in the random-dots task compared to instructed saccade task.*

workspace (relative to head-position), and to the right in the other (Figure 6a, "left" and "right" workspaces). The location corresponding to the center of the monitor could thus either be the target of a rightward or a leftward saccade.

Using a single decoder that has no information about gaze-location we can decode the direction of the rewarded saccade with high accuracy throughout the central-fixation, movement, and target-fixation periods (Figure 6a, right panel).

At the level of individual units, gaze-location also does not appear to strongly modulate saccade related activity. We quantified the influence of saccade direction and gaze location with a linear regression model, whereby each unit's activity is captured as a combination of these two factors. Across all units, the previous saccade direction explained a much bigger portion of the variance than gaze-location (Figure 6b; Suppl. Fig. 6f, l other monkeys).

The different decoding accuracy across the different types of saccades in the instructed saccade task (Figure 3a and Figure 5a) thus are not explained by effects of gaze location, nor can they be accounted for by differences in the distribution of saccade directions across saccade types (Suppl. Fig. 7a). The different accuracies may imply that post-saccadic activity is modulated by contextual influences like the temporally discounted reward-expectation[31], which differs across saccade types.

Post-saccadic activity is modulated by task demands

To study more explicitly if task context can affect post-saccadic representations, we compared the post-saccadic activity of rewarded saccades in monkey T across two tasks that place different demands on the activity bridging actions and rewards: an instructed saccade task, analogous to that in Figure 1, and a motion-discrimination task. Both tasks required saccades to only one of two targets, placed at identical locations across tasks (Figure 6c, left panel, dots vs. instructed saccade task). In the instructed saccade task, a saccade to the single presented target was always rewarded. In contrast, the discrimination task required a choice between two targets based on previously presented sensory information, and not all saccades to the chosen target were rewarded. Validating past choices, and if necessary adjusting the employed strategies[71–76], would then require at the time of feedback a representation of the immediately preceding stimuli and actions.

To ascertain the representation of the preceding actions across the two tasks, we compared decoding accuracy for the direction of the rewarded saccade. Decoding accuracy was high for both tasks (Figure 6c, right panel). Notably, the same set of time-dependent decoders resulted in high-accuracy read-outs in both tasks, indicating that the pre and post-saccadic representation was similar in the two scenarios. The strength of post-saccadic activity, but not of pre-saccadic activity, was however reduced for instructed eye movements compared to decision-driven eye movements in both monkey T and monkey V (Figure 6c,d).

In summary, while post-saccadic activity appears to be maintained in PFC for varying durations after every saccade (instructed or free, rewarded or un-rewarded), its strength appears to be contextually modulated—post-saccadic activity is strongest after saccades expected to lead to a reward, and in a setting requiring the monkeys to adapt their behavior based on the collected rewards.

Pre-saccadic and post-saccadic representations have different dynamics

Cross-temporal decoding of saccade direction suggests a prominent difference between pre- and post-saccadic representations: pre-saccadic encoding appears to be stable, whereas post-saccadic encoding is dynamic (Figure 3b, compare the “block” structure at bottom-left to the diagonal pattern in the middle). Decoding matrices such as those in Figure 3b are obtained by averaging decoder outcomes over many trials. On single trials, however, population dynamics also reflects processes not locked to saccade initiation, and could differ from averaged dynamics. In the following, we thus investigate how the differences between average pre- and post-saccadic dynamics are reflected in single trials (Figure 7).

In contrast to the analyses in Figure 3, we will now consider single-trial decoding matrices that contain the decoding error, a continuous measure of decoding accuracy on single trials (Suppl. Fig. 8b), rather than the decoding success as in Figure 3 (i.e. correct vs. wrong direction). The decoding error, defined as the unsigned difference between the actual and predicted saccade direction, ranges between 0 and 180 degrees and allows for a finer mapping of the dynamics of saccade representations: small decoding errors can capture representations that become corrupted by noise over time or drift[77], whereas larger decoding errors can capture large, systematic transitions in the representations, e.g. to orthogonal or inverted subspaces of the activity.

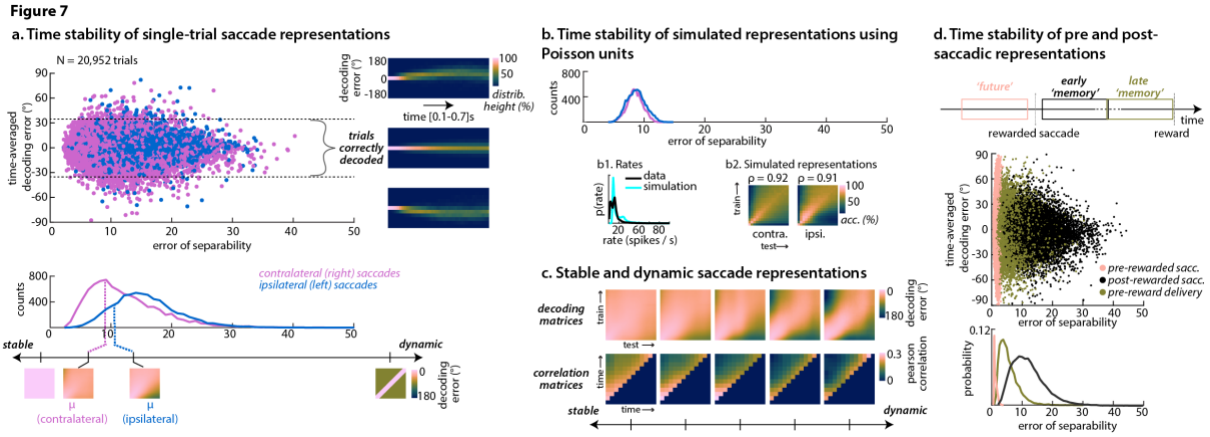

Figure 7. ***Single-trial dynamics of saccade representations****. Data from the visually-guided saccade task, as in Figure 3. Decoders are trained and evaluated on the direction of the rewarded saccade.* ***a.*** *Time stability of saccade representations (dynamic or static), quantified as the difference between the measured decoding matrix and its separable approximation ("error of separability"). Single-trial decoding matrices are constructed based on the cross-temporal decoding error (Supplementary Figure 8b). Top-left: error of separability vs. decoding error for individual trials (points; color: saccade laterality). Decoding error was averaged across all the time-specific post-saccadic decoders (diagonal values in the decoding matrix). Small and large errors of separability are indicative of static and dynamic representations, respectively. Top-right: histograms of time-dependent decoding errors for well (middle) and poorly decoded trials (top and bottom). Bottom histogram of error of separability, separately by saccade laterality (rightward and leftward saccades). Example decoding matrices corresponding to extreme (left and right) and average errors of separability (μ) are shown below the horizontal axis.* ***b.*** *Error-of-separability in simulated population responses based on Poisson variability (Supplementary Figure 9). The simulated and measured responses are matched in rates (b1) and average cross-temporal decoding matrices (b2). The resulting errors of separability are distributed narrowly around the mean (top, compare to a), indicating that the simulated single-trial decoding matrices closely resemble the average decoding matrix.* ***c.*** *Top: single-trial decoding matrices, sorted and averaged based on the error of separability. Bottom: single-trial cross-temporal correlation matrices (vertical and horizontal axis indicate time in trial), sorted and averaged based on error of separability. Diagonal values are removed, since they trivially only contain '1's. Both decoding and correlation matrices reveal a continuum of trials ranging from stable to strongly dynamic. Only trials correctly decoded are included (see a).* ***d.*** *Error of separability, for decoding matrices from three different time-windows (each 0.6s long): pre-rewarded saccade, post-rewarded saccade and pre-reward delivery. Saccade representations are consistently separable (small errors) before the saccade ('future') but not after the saccade (early 'memory') or before the reward delivery (late 'memory').*

The time-course of these single-trial decoding errors can be used to distinguish stable and dynamic encoding on single trials. Stable encoding implies that a fixed, single decoder is optimal at each time within the considered epoch. Decoding error could nonetheless vary throughout the epoch even for stable encoding, if the strength of the encoded signal is modulated over time—errors from the optimal decoder would be small when the signal is strong, and larger when it is weak. Notably, the same modulation of decoding errors would typically be apparent also in the read-outs of non-optimal decoders, as it simply reflects the relative strength of signal and noise.

The decoding matrix of a stationary pattern can, therefore, be separated into the product of two temporal profiles v_1 and u_1 (similar to how space-time separability in receptive fields can be measured[78], Suppl. Fig. 8a, b), where v_1 (horizontal axis) describes how the strength of saccade-related activity is modulated throughout the trial, and u_1 (vertical axis) describes which of the trained decoders is optimal for that trial. In contrast, a non-stationary pattern requires different decoders at different times. The corresponding decoding matrix is dynamic

and cannot be separated in this fashion. Thus, small errors between the original matrix and the separable approximation imply stable encoding, whereas large errors are more consistent with dynamic encoding.

The errors of separability for early post-saccadic activity are distributed over a surprisingly wide range of values (Figure 7a). Different trials from the same task-condition (saccade direction and eccentricity) can result in diverse errors of separability—some trials have errors close to zero, implying stable encoding, whereas others have large errors, implying dynamic encoding (Suppl. Fig. 8c). This diversity is not explained by differences in decoding accuracy, as it can be observed even among trials that are very well decoded (Figure 7a, middle section: 'trials correctly decoded').

To better illustrate the diversity in single-trial dynamics, we grouped and averaged trials according to their error of separability (Figure 7c). The resulting average decoding matrices range from largely static to strongly dynamic, validating our definition of the error of separability (Figure 7c, top row). The different types of single-trial dynamics can be appreciated even when considering the population responses directly (Figure 7c, bottom row). We computed cross-temporal correlation matrices, whereby each entry represents the linear correlation between population responses from different times in the trial. Sorting these single-trial correlation matrices according to the error of separability again revealed the same gradual transition from 'block'-like to 'diagonal'-like structure.

The observed diversity in encoding dynamics is not explained by spiking variability in single units, as shown by simulations that combine the measured, condition-averaged responses of single units with trial-by-trial variability drawn from a Poisson distribution (Figure 7b). By design, the simulated population responses capture the *average* decoding matrices (Figure 7b1 and b2) and, as a result, the average error of separability. Dynamic encoding in these simulations stems from both time-dependent preferred direction in single neurons, as well as variation in the time of peak-selectivity across neurons (Suppl. Fig. 9), two effects that appear insufficient to explain the full spectrum of dynamics of post-saccadic activity observed on single trials.

Finally, we tested if the prominent difference between pre- and post-saccadic encoding exists on single trials by comparing the error of separability across three epochs: pre-saccadic, early post-saccadic and late post-saccadic (Figure 7d). Reflecting the differences from the average decoding matrices (Suppl. Fig 8d), we find that single-trial decoding matrices are consistently separable during the pre-saccadic epoch (Figure 7d, pink) but can deviate strongly from the separable approximation in the post-saccadic epoch, more so in the early vs. the late epoch (Figure 7d, black and green), interestingly with a few exceptions (Figure 7d, error close to zero). Overall, these analyses of single trials corroborate the finding that, in this task, pre-saccadic and post-saccadic responses differ substantially in the nature of their representations, and thus potentially in their underlying neural mechanisms.

Discussion

We measured population activity in pre-arcuate cortex of macaque monkeys in a classic oculomotor task (visually guided, delayed saccades) as well as a perceptual decision-making task. We applied population decoding in combination with analyses of single-unit activity to obtain a precise characterization post-saccadic activity in pre-arcuate cortex.

Properties of post-saccadic activity

We find that post-saccadic activity is the strongest and most prominent form of saccade-related activity, both at the level of single cells (Figure 2) and at the population level (Figure 3). The direction of the rewarded saccade can be best decoded after the saccade is already completed, and decoding performance remains high until the time of feedback, throughout a delay period during which the gaze is fixated (Figure 3a).

This persistence seems at odds with the findings of some previous studies, which instead reported largely transient post-saccadic activity[9,46]. These past studies, however, did not include a temporal separation between the saccade and the feedback. The persistent nature of post-saccadic activity might become apparent only when such a delay period is included in the task, since it requires the active maintenance of saccade-related information until feedback is provided.

As in more posterior areas of PFC[9,28,44,45], but not more anterior ones[79,80], post-saccadic activity is intermingled with pre-saccadic and movement related activity. While many cells with pre-saccadic activity do also show post-saccadic activity, a large population of units show exclusively post-saccadic activity (Figure 4b; Suppl. Fig. 3a, f). These units thus appear not involved in the selection, preparation, or execution of the upcoming saccade[9,28,44,45]. In this sense, post-saccadic representations in pre-arcuate cortex appear to differ substantially from proposed encoding schemes that rely on mixed selectivity, whereby various task-related signals are mixed randomly in the activity of single cells[33,59].

Both at the level of single cells and at the population level, saccadic representations undergo a prominent, long-lasting "flip" at the time of each saccade (Figure 3c, Figure 5b, Suppl. Fig 5). This flip is driven by neurons that are selective for direction both before and after the saccade—in such neurons, the preferred direction typically flips by 180 degrees between the pre- and post-saccadic epochs in a highly structured manner, inconsistent with mixed selectivity (Figure 4c). Critically, we find strong evidence that this flip does not reflect a movement plan for a saccade back to the point of origin of the previous saccade: we observed the same flip for all types of saccades we analyzed (Figure 5b; Figure 5c), and post-saccadic activity alone is not predictive of the direction of the upcoming saccade (Figure 5b; Suppl. Fig. 6c, i). Analogous flips in selectivity have been observed before in relation to saccades[9,28], but may also occur in other settings[62,81]. As discussed below, one possible function of the observed flips may be to update a representation of visual space across saccades.

Both pre-saccadic[28] and post-saccadic representations reflect retinotopic coordinates. Like other types of movements, saccades could in principle be represented in a variety of alternative coordinate systems, from head-centered, to body-centered, and world-centered coordinates[82,83]. Like past studies in dorso-lateral prefrontal cortex[28,84], we, however, find no evidence for representations of saccades in coordinate systems other than retinotopic coordinates (Figure 6a, b; Suppl. Fig 6f, l). Potential candidate structures for such representations in other coordinate systems involve hippocampal areas and parts of PFC closely linked to it[85–89].

Unlike pre-saccadic activity[28,44,50,90] (but see[91]), post-saccadic activity occurs after every saccade. However, it was strongest, and lasted the longest following "rewarded" saccades, i.e. the last saccades preceding feedback and reward delivery (Figure 3a). Weaker and more short-lived post-saccadic activity followed the start saccades that initiated a trial, and the end-

saccades that followed the reward (Figure 5a). We also observed stronger post-saccadic activity in the perceptual discrimination task compared to the instructed-saccade task. This modulation by task context may reflect differences in reward predictability (80% and 100% correct trials in the two tasks, respectively) or different demands for action memories in the two tasks.

Possible functions of post-saccadic activity

The properties of post-saccadic activity in pre-arcuate cortex appear inconsistent with a number of proposed hypotheses about its function[46]. Since post-saccadic activity is not predictive of the next saccade, it is unlikely to represent a plan for a future action (see also[28]). A hypothesized role in "resetting" activity in PFC, to set the stage for a new saccade plan[46], seems at odds with the observation that post-saccadic activity can persist over long temporal intervals. This persistence, together with a pronounced context dependency, also rules out the possibility that post-saccadic activity represents a corollary discharge for saccades. Instead, post-saccadic activity could represent an action memory contributing to learning[3,41,42,80,92].

Many reinforcement learning algorithms[47] use eligibility traces, i.e. temporary records of previous actions, to evaluate the actions' relevance with respect to rewards[37,80,93–96]. Eligibility traces of eye movements are particularly important for learning, as eye movements provide a fast feedback of motor performance[97,98]. Implementing such algorithms in neural circuits is challenging, as learning may rely on biophysical mechanisms like spike-timing dependent plasticity (STDP) that operate on much shorter times-scales than the task-events relevant for behavior[99,100]. Past proposals on how to link synaptic plasticity to times-scale of behavior include tagging synapses to make them eligible for future reinforcement-driven changes[101,102] or prolonging the temporal footprint of STDP[103,104]. Such mechanisms seem ill-suited to the tasks studied here, as the duration of the target-fixation period separating action and outcome outlasts even the longest-documented windows of adult-brain STDP[105]. On the other hand, by actively representing an action-memory as persistent activity in the network, representations of actions and rewards that are separated in time might be made to temporally overlap in the brain, thus allowing learning to occur through fast mechanisms like STDP. Our finding that post-saccadic activity is modulated by saccade type and task may imply that action memories, similarly to working memory of sensory information, are maintained in PFC flexibly, and preferentially for those actions that are most relevant for learning. Such action memories may complement or interact with alternative mechanisms that could allow task-relevant signals to be maintained without persistent activity[106], such as an 'activity-silent' memory emerging from changes in synaptic efficacy[107,108].

The finding that saccades are dynamically encoded in post-saccadic activity echoes past reports of choice memories represented as sequences of activity in rodent prefrontal and parietal cortex[109–112]. Neurons engaged by such choice sequences were found to project to the striatum[110], an area important for associative learning, thus making them plausible candidates for maintaining eligibility traces. The post-saccadic activity we report here, however, differs in some respects from previously reported choice related sequences. First, we show that post-saccadic activity appears to follow every saccade, not just saccadic movements related to a choice between learned alternatives. Second, post-saccadic activity, while dynamic, nonetheless changes smoothly as saccades direction is varied along a circle

and in this sense may be amenable to a description in terms of single-unit response fields. Third, we observe post-saccadic activity during fixation periods in which task-relevant movements are suppressed, effectively excluding possible explanations of this activity through movement confounds[113].

Beyond maintaining an action memory, post-saccadic activity could contribute to updating representations of visual space in PFC and to maintaining visual stability across saccades[45,114,115]. Our own work and previous studies show that visual stimuli, salient locations, action-plans, and action memories are all represented in dlPFC in maps organized in retinotopic coordinates[28,45,50]. Any behavior requiring more than a single saccade, like the visual exploration of a scene, or the execution of sequences of saccades to multiple remembered locations, requires updating these retinotopic maps following each saccade. Concretely, after a saccade, a retinotopic map needs to be updated by shifting it along a vector that is the exact *opposite* of the vector of the saccade that was just executed (Suppl. Fig. 10 and Fig. 13 in [45]). The prominent flip in direction selectivity observed after each saccade could provide such an update signal, or could reflect the outcome of the update process. Past work has suggested that adjusting sensory representations using an internal copy of the previous saccade may be advantageous compared to alternative mechanisms that appear to be slower[116].

This interpretation of post-saccadic activity as computing updates of spatial representations would imply a critical role for PFC in predicting and compensating for the consequences of one's own actions[114,115,118]. Consistent with such a role, impairments in generating and incorporating predictions are thought to be a defining feature of schizophrenia[119,120], which consistently involves prominent changes in prefrontal circuits[120,121] as well as an impaired ability to generate long and frequent saccades in visual exploration[122].

Finally, post-saccadic activity could also contribute to updating upcoming motor plans of other motor effectors[98]. Tracking the eye movements in daily activities revealed that anticipatory saccades precede perfected skills[117]. Given that eye movements are among the fastest motor responses, the delay between seeing and doing could be a computational shortcut. One intriguing possibility is that the anticipatory saccade is part of the learned procedure and acts as a 'go-cue' to the learned motor sequence to speed-up reaction times (see[10] for a review of procedural learning). Whether a sustained representation of this anticipatory saccade would facilitate the execution of motor sequences remains an open question.

Planning vs. remembering an action

The mechanisms underlying pre- and post-saccadic activity may be substantially different. Both on average and on single trials, pre-saccadic persistent activity is stable, involving activation of a fixed pattern of activation across the population (Figure 7d, "future"). Such stable representations are consistent with so-called attractor dynamics[123–125] and are observed even in memory-based saccade tasks, where activity cannot be stabilized by a tonic visual input[57]. Post-saccadic activity, on the other hand, is dynamic on average and for the majority of single trials (Figure 7d, early and late "memory"), implying that the saccade representation is likely carried by a temporal sequence of many activity patterns across the population[126,127]. The representation remains dynamic even for the longest target-fixation intervals we considered, up to the time immediately preceding the feedback and the delivery

of reward. Such sequential, dynamic representations, which are inconsistent with attractor dynamics[128], have been observed in other species and areas, albeit often on slower time-scales[111,127]. Activity representing the *plan* of an action may need to be constrained into specific state-space locations, to avoid the premature execution of the movement, to allow fast reaction times and accurate movements[64,129], and to avoid interference with future goals[130]. Such constraints may not apply to the *memory* of an action, in particular if, as in our recordings, that memory is carried also by a dedicated population of neurons that is not involved in planning and executing the movement.

The apparent discrepancy between how a saccade is encoded before and after its execution raises the question of whether these differences are generated within prefrontal recurrent circuits, or are inherited through inputs or feedback from other areas. Further insights into the circuit mechanisms underlying these two types of activity could advance our understanding of how plans are transformed into memories along the prefrontal hierarchical network.

Conclusion

Pre-arcuate cortex actively maintains accurate, persistent representations of saccades before, during, and after each saccadic movement. The representations of future and past saccades involve different patterns of population activity and largely distinct groups of single neurons. Despite their different neural substrates, saccadic action plans and saccadic action memories are represented in the same frame of reference, retinotopic coordinates, making them well-suited as a basis for reinforcement learning algorithms[47] and for the computations underlying visual stability across saccades[114]. The observed, prominent representations of saccadic action memories support a prominent role of PFC in linking events across time, and may provide the basis for more abstract, choice-related mnemonic representations throughout the brain[79,80,131,132].

Authors Contribution

I.C. and V.M. designed the study and the methods. J.R. conceived and conducted the experiments and collected the data. I.C. performed the analyses, with input from V.M. and assistance from S.K. S.K. provided software for data visualisation and data pre-processing. I.C., V.M. and S.K. wrote the manuscript. All authors were involved in discussing the results and the manuscript.

Acknowledgments

We thank W. T. Newsome for the data collection and discussions on the results. We also thank members of the Mante Lab for valuable feedback throughout the project.

Funding

This work was supported by the Swiss National Science Foundation (SNSF Professorship PP00P3-157539, VM), the Simons Foundation (award 328189 to W. T. Newsome and V.M., and 543013 to V.M.), the Swiss Primate Competence Center in Research, the Howard Hughes Medical Institute (through W. T. Newsome) and the DOD | USAF | AFMC | Air Force Research Laboratory: W. T. Newsome, agreement number FA9550-07-1-0537 (VM and JR).

References

1. Koechlin, E., Ody, C. & Kouneiher, F. The Architecture of Cognitive Control in the Human Prefrontal Cortex. *Science (80-.).* **302**, 1181–1185 (2003).
2. Fuster, J. M. Upper processing stages of the perception–action cycle. *Trends Cogn. Sci.* **8**, 143–145 (2004).
3. Tsujimoto, S., Genovesio, A. & Wise, S. P. Frontal pole cortex: Encoding ends at the end of the endbrain. *Trends Cogn. Sci.* **15**, 169–176 (2011).
4. Chen, L. L. & Wise, S. P. Neuronal Activity in the Supplementary Eye Field During Acquisition of Conditional Oculomotor Associations. *J. Neurophysiol.* **73**, (1995).
5. Nakamura, K., Sakai, K. & Hikosaka, O. Neuronal activity in medial frontal cortex during learning of sequential procedures. *J. Neurophysiol.* **80**, 2671–2687 (1998).
6. Sakai, K. *et al.* Transition of Brain Activation from Frontal to Parietal Areas in Visuomotor Sequence Learning. *J. Neurosci.* **18**, 1827–1840 (1998).
7. Funahashi, S., Bruce, C. J. & Goldman-Rakic, P. S. Mnemonic coding of visual space in the monkey's dorsolateral prefrontal cortex. *J. Neurophysiol.* **61**, 331–349 (1989).
8. FUNAHASHI, S., TAKEDA, K. & WATANABE, Y. Neural mechanisms of spatial working memory: Contributions of the dorsolateral prefrontal cortex and the thalamic mediodorsal nucleus. *Cogn. Affect. Behav. Neurosci.* **4**, 409–420 (2004).
9. Funahashi, S., Bruce, C. J. & Goldman-Rakic, P. S. Neuronal activity related to saccadic eye movements in the monkey's dorsolateral prefrontal cortex. *J. Neurophysiol.* **65**, 1464–1483 (1991).
10. Hikosaka, O. *et al.* Parallel neural networks for learning sequential procedures. *Trends Neurosci.* **22**, 464–471 (1999).
11. Petersen, S. E., Mier, H. van, Fiez, J. A. & Raichle, M. E. The effects of practice on the functional anatomy of task performance. *Proc. Natl. Acad. Sci.* **95**, 853–860 (1998).
12. Grafton, S. T. *et al.* Functional Anatomy of Human Procedural Learning Determined with Regional Cerebral Blood Flow and PET. *J. Neurosci.* 2542–2548 (1992).
13. Szczepanski, S. M. & Knight, R. T. Insights into human behavior from lesions to the prefrontal cortex. *Neuron* **83**, 1002–18 (2014).
14. Buckley, M. J. *et al.* Dissociable components of rule-guided behavior depend on distinct medial and prefrontal regions. *Science* **325**, 52–58 (2009).
15. Mansouri, F. A., Buckley, M. J. & Tanaka, K. Mnemonic function of the dorsolateral prefrontal cortex in conflict-induced behavioral adjustment. *Science* **318**, 987–990 (2007).
16. Duncan, J. Disorganisation of Behaviour After Frontal Lobe Damage. *Cogn. Neuropsychol.* **3**, 271–290 (1986).
17. Grafman, J. Plans, actions, and mental sets: Managerial knowledge units in the frontal lobes. in *Integrating Theory and Practice in Clinical Neuropsychology* 93–138 (Taylor and Francis, 1989). doi:10.4324/9780429489464-4

18. Miller, E. K. & Cohen, J. D. An Integrative Theory of Prefrontal Cortex Function. *Annu. Rev. Neurosci.* **24**, 167–202 (2001).

19. Tanji, J. & Hoshi, E. Role of the Lateral Prefrontal Cortex in Executive Behavioral Control. *Physiol. Rev.* **88**, 37–57 (2008).

20. Averbeck, B. B., Sohn, J. W. & Lee, D. Activity in prefrontal cortex during dynamic selection of action sequences. *Nat. Neurosci.* **9**, 276–282 (2006).

21. Averbeck, B. B. & Lee, D. Prefrontal Neural Correlates of Memory for Sequences. (2007). doi:10.1523/JNEUROSCI.4483-06.2007

22. Romo, R., Brody, C. D., Hernández, A. & Lemus, L. Neuronal correlates of parametric working memory in the prefrontal cortex. *Nature* **399**, 470–473 (1999).

23. Rao, S. C., Rainer, G. & Miller, E. K. Integration of what and where in the primate prefrontal cortex. *Science* **276**, 821–4 (1997).

24. Asaad, W. F., Lauro, P. M., Perge, J. A. & Eskandar, E. N. Prefrontal neurons encode a solution to the credit-assignment problem. *J. Neurosci.* **37**, 6995–7007 (2017).

25. Gitelman, D. R. *et al.* A large-scale distributed network for covert spatial attention. *Brain* **122**, 1093–1106 (1999).

26. Hanks, T. D. *et al.* Distinct relationships of parietal and prefrontal cortices to evidence accumulation. *Nature* **520**, 220–223 (2015).

27. Shadlen, M. N. & Newsome, W. T. Neural Basis of a Perceptual Decision in the Parietal Cortex (Area LIP) of the Rhesus Monkey. *J. Neurophysiol.* **86**, 1916–1936 (2001).

28. Bruce, C. J. & Goldberg, M. E. Primate frontal eye fields. I. Single neurons discharging before saccades. *J. Neurophysiol.* **53**, 603–35 (1985).

29. Watanabe, M. Reward expectancy in primate prefrontal neurons. *Nature* **382**, 629–632 (1996).

30. Teichert, T., Yu, D. & Ferrera, V. P. Performance monitoring in monkey frontal eye field. *J. Neurosci.* **34**, 1657–71 (2014).

31. Kim, S., Hwang, J. & Lee, D. Prefrontal Coding of Temporally Discounted Values during Intertemporal Choice. *Neuron* **59**, 161–172 (2008).

32. Rigotti, M., Rubin, D. B. D., Wang, X. J. & Fusi, S. Internal representation of task rules by recurrent dynamics: The importance of the diversity of neural responses. *Front. Comput. Neurosci.* **4**, 24 (2010).

33. Mante, V., Sussillo, D., Shenoy, K. V. & Newsome, W. T. Context-dependent computation by recurrent dynamics in prefrontal cortex. *Nature* **503**, 78–84 (2013).

34. Barak, O., Tsodyks, M. & Romo, R. Neuronal population coding of parametric working memory. *J. Neurosci.* **30**, 9424–9430 (2010).

35. Yang, G. R., Joglekar, M. R., Song, H. F., Newsome, W. T. & Wang, X. J. Task representations in neural networks trained to perform many cognitive tasks. *Nat. Neurosci. 2019 222* **22**, 297–306 (2019).

36. Wong, K. F. & Wang, X. J. A Recurrent Network Mechanism of Time Integration in

668 Perceptual Decisions. *J. Neurosci.* **26**, 1314–1328 (2006).

669 37. Lee, D., Seo, H. & Jung, M. W. Neural Basis of Reinforcement Learning and Decision
670 Making. *Annu. Rev Neurosc.* **35**, 287–308 (2012).

671 38. Kable, J. W. & Glimcher, P. W. The Neurobiology of Decision: Consensus and
672 Controversy. *Neuron* **63**, 733 (2009).

673 39. Hanks, T. D. & Summerfield, C. Perceptual Decision Making in Rodents, Monkeys, and
674 Humans. *Neuron* **93**, 15–31 (2017).

675 40. Barraclough, D. J., Conroy, M. L. & Lee, D. Prefrontal cortex and decision making in a
676 mixed-strategy game. *Nat. Neurosci.* **7**, (2004).

677 41. Donahue, C. H. & Lee, D. Dynamic routing of task-relevant signals for decision making
678 in dorsolateral prefrontal cortex. *Nat. Neurosci.* **18**, 295–301 (2015).

679 42. Seo, H., Barraclough, D. J. & Lee, D. Dynamic Signals Related to Choices and Outcomes
680 in the Dorsolateral Prefrontal Cortex. *Cereb. Cortex* **17**, i110–i117 (2007).

681 43. Tsutsui, K. I., Grabenhorst, F., Kobayashi, S. & Schultz, W. A dynamic code for economic
682 object valuation in prefrontal cortex neurons. *Nat. Commun.* **7**, 1–16 (2016).

683 44. Bizzi, E. Discharge of frontal eye field neurons during saccadic and following eye
684 movements in unanesthetized monkeys. *Exp. Brain Res.* **6**, 69–80 (1968).

685 45. Goldberg, M. E. & Bruce, C. J. Primate frontal eye fields. III. Maintenance of a spatially
686 accurate saccade signal. *J. Neurophysiol.* **64**, 489–508 (1990).

687 46. Funahashi, S. Saccade-related activity in the prefrontal cortex: its role in eye movement
688 control and cognitive functions. *Front. Integr. Neurosci.* **8**, 54 (2014).

689 47. Sutton, R. S., Barto, A. G. & Book, A. B. Reinforcement Learning: An Introduction.
690 (2017).

691 48. Sommer, M. A. & Wurtz, R. H. Composition and topographic organization of signals
692 sent from the frontal eye field to the superior colliculus. *J. Neurophysiol.* **83**, 1979–2001
693 (2000).

694 49. Takeda, K. & Funahashi, S. Prefrontal Task-Related Activity Representing Visual Cue
695 Location or Saccade Direction in Spatial Working Memory Tasks. (2002).
696 doi:10.1152/jn.00249.2001

697 50. Bruce, C. J., Goldberg, M. E., Bushnell, M. C. & Stanton, G. B. Primate frontal eye fields.
698 II. Physiological and anatomical correlates of electrically evoked eye movements. *J.*
699 *Neurophysiol.* **54**, 714–734 (1985).

700 51. Funahashi, S., Chafee, M. & Goldman-Rakic, P. Prefrontal neuronal activity in rhesus
701 monkeys performing a delayed anti-saccade task. *Nature* **365**, 753–756 (1993).

702 52. Bullock, K. R., Pieper, F., Sachs, A. J. & Martinez-Trujillo, J. C. Visual and presaccadic
703 activity in area 8Ar of the macaque monkey lateral prefrontal cortex. *J. Neurophysiol.*
704 **118**, 15–28 (2017).

705 53. Kim, J.-N. & Shadlen, M. N. Neural correlates of a decision in the dorsolateral prefrontal
706 cortex of the macaque. *Nat. Neurosci.* **2**, 176–185 (1999).

54. Khaki, M., LUNA, R., MORTAZAVI, N., SACHS, A. & MARTINEZ-TRUJILLO, J. Using classification-based decoding to analyze the Spatiotopic and Retinotopic memory representations in primates. *J. Vis.* **21**, 2868–2868 (2021).

55. Luna, R. *et al.* Small neuronal ensembles of primate lateral prefrontal cortex encode spatial working memory in two reference frames. *J. Vis.* **21**, 2858–2858 (2021).

56. Almeida, R. L., Roussy, M. P., Sachs, A., Treue, S. & Martinez-Trujillo, J. C. Neuronal ensembles of primate Lateral Prefrontal Cortex encode spatial working memory in different frames of reference. *J. Vis.* **20**, 1753–1753 (2020).

57. Stokes, M. G. *et al.* Dynamic coding for cognitive control in prefrontal cortex. *Neuron* **78**, 364–75 (2013).

58. Parthasarathy, A. *et al.* Mixed selectivity morphs population codes in prefrontal cortex. *Nat. Neurosci.* **20**, 1770–1779 (2017).

59. Rigotti, M. *et al.* The importance of mixed selectivity in complex cognitive tasks. *Nature* **497**, 585–590 (2013).

60. Spaak, E., Watanabe, K., Funahashi, S. & Stokes, M. G. Stable and dynamic coding for working memory in primate prefrontal cortex. *J. Neurosci.* **37**, 6503–6516 (2017).

61. Murray, J. D. *et al.* Stable population coding for working memory coexists with heterogeneous neural dynamics in prefrontal cortex. *Proc. Natl. Acad. Sci. U. S. A.* **114**, 394–399 (2017).

62. Khanna, S. B., Scott, J. A. & Smith, M. A. Dynamic shifts of visual and saccadic signals in prefrontal cortical regions 8Ar and FEF. *J. Neurophysiol.* **124**, 1774–1791 (2020).

63. Tang, C., Herikstad, R., Parthasarathy, A., Libedinsky, C. & Yen, S. C. Minimally dependent activity subspaces for working memory and motor preparation in the lateral prefrontal cortex. *Elife* **9**, 1–23 (2020).

64. Elsayed, G. F., Lara, A. H., Kaufman, M. T., Churchland, M. M. & Cunningham, J. P. Reorganization between preparatory and movement population responses in motor cortex. *Nat. Commun. 2016 71* **7**, 1–15 (2016).

65. Churchland, M. M. & Shenoy, K. V. Temporal Complexity and Heterogeneity of Single-Neuron Activity in Premotor and Motor Cortex. *J. Neurophysiol.* **97**, 4235–4257 (2007).

66. Andersen, R. & Mountcastle, V. The influence of the angle of gaze upon the excitability of the light- sensitive neurons of the posterior parietal cortex. *J. Neurosci.* **3**, 532–548 (1983).

67. Brotchie, P. R., Andersen, R. A., Snyder, L. H. & Goodman, S. J. Head position signals used by parietal neurons to encode locations of visual stimuli. *Nature* **375**, 232–235 (1995).

68. Andersen, R. A., Essick, G. K. & Siegel, R. M. Encoding of spatial location by posterior parietal neurons. *Science (80-.).* **230**, 456–458 (1985).

69. RA, A., RM, B., S, B., JW, G. & L, F. Eye position effects on visual, memory, and saccade-related activity in areas LIP and 7a of macaque. *J. Neurosci.* **10**, 1176–1196 (1990).

70. Salinas, E. & Abbott, L. F. Chapter 11 Coordinate transformations in the visual system:

how to generate gain fields and what to compute with them. *Prog. Brain Res.* **130**, 175–190 (2001).

71. Pouget, A., Drugowitsch, J. & Kepecs, A. Confidence and certainty: distinct probabilistic quantities for different goals. *Nat. Neurosci. 2016 193* **19**, 366–374 (2016).

72. Purcell, B. A. & Kiani, R. Neural Mechanisms of Post-error Adjustments of Decision Policy in Parietal Cortex. *Neuron* **89**, 658–71 (2016).

73. Kerns, J. G. *et al.* Anterior cingulate conflict monitoring and adjustments in control. *Science* **303**, 1023–1026 (2004).

74. Mansouri, F. A., Tanaka, K. & Buckley, M. J. Conflict-induced behavioural adjustment: a clue to the executive functions of the prefrontal cortex. *Nat. Rev. Neurosci.* **10**, 141–152 (2009).

75. Rouault, M., Drugowitsch, J. & Koechlin, E. Prefrontal mechanisms combining rewards and beliefs in human decision-making. *Nat. Commun. 2019 101* **10**, 1–16 (2019).

76. Drugowitsch, J., Moreno-Bote, R. N., Churchland, A. K., Shadlen, M. N. & Pouget, A. The Cost of Accumulating Evidence in Perceptual Decision Making. *J. Neurosci.* **32**, 3612–3628 (2012).

77. Wolff, M. J., Jochim, J., Akyürek, E. G., Buschman, T. J. & Stokes, M. G. Drifting codes within a stable coding scheme for working memory. *PLOS Biol.* **18**, e3000625 (2020).

78. DeAngelis, G. C., Ohzawa, I. & Freeman, R. D. Receptive-field dynamics in the central visual pathways. *Trends Neurosci.* **18**, 451–458 (1995).

79. Tsujimoto, S., Genovesio, A. & Wise, S. P. Monkey orbitofrontal cortex encodes response choices near feedback time. *J. Neurosci.* **29**, (2009).

80. Tsujimoto, S., Genovesio, A. & Wise, S. P. Evaluating self-generated decisions in frontal pole cortex of monkeys. *Nat. Neurosci. 2009 131* **13**, 120–126 (2010).

81. Libby, A. & Buschman, T. J. Rotational dynamics reduce interference between sensory and memory representations. *Nat. Neurosci.* **24**, 715–726 (2021).

82. Andersen, R. A., Snyder, L. H., Bradley, D. C. & Xing, J. Multimodal representation of space in the posterior parietal cortex and its use in planning movements. *Annu. Rev. Neurosci.* **20**, 303–330 (1997).

83. Snyder, L. H. Coordinate transformations for eye and arm movements in the brain. *Curr. Opin. Neurobiol.* **10**, 747–754 (2000).

84. Golomb, J. D., Chun, M. M. & Mazer, J. A. The native coordinate system of spatial attention is retinotopic. *J. Neurosci.* **28**, 10654–10662 (2008).

85. Meister, M. L. R. & Buffalo, E. A. Neurons in Primate Entorhinal Cortex Represent Gaze Position in Multiple Spatial Reference Frames. *J. Neurosci.* **38**, 2430–2441 (2018).

86. Killian, N. J., Potter, S. M. & Buffalo, E. A. Saccade direction encoding in the primate entorhinal cortex during visual exploration. *Proc. Natl. Acad. Sci. U. S. A.* **112**, 15743–15748 (2015).

87. Meister, M. L. R. & Buffalo, E. A. Getting directions from the hippocampus: The neural

786 connection between looking and memory. *Neurobiol. Learn. Mem.* **134 Pt A**, 135–144
787 (2016).

788 88. Baram, A. B., Muller, T. H., Nili, H., Garvert, M. M. & Behrens, T. E. J. Entorhinal and
789 ventromedial prefrontal cortices abstract and generalize the structure of
790 reinforcement learning problems. *Neuron* **109**, 713-723.e7 (2021).

791 89. Garvert, M. M., Dolan, R. J. & Behrens, T. E. J. A map of abstract relational knowledge
792 in the human hippocampal–entorhinal cortex. *Elife* **6**, (2017).

793 90. Bizzi, E. & Schiller, P. H. Single unit activity in the frontal eye fields of unanesthetized
794 monkeys during eye and head movement. *Exp. Brain Res.* **10**, 151–158 (1970).

795 91. Sendhilnathan, N., Basu, D., Goldberg, M. E., Schall, J. D. & Murthy, A. Neural correlates
796 of goal-directed and non-goal-directed movements. *Proc. Natl. Acad. Sci. U. S. A.* **118**,
797 2021 (2021).

798 92. Curtis, C. E. & Lee, D. Beyond working memory: The role of persistent activity in
799 decision making. *Trends Cogn. Sci.* **14**, 216–222 (2010).

800 93. Koechlin, E. Prefrontal executive function and adaptive behavior in complex
801 environments. *Curr. Opin. Neurobiol.* **37**, 1–6 (2016).

802 94. Averbeck, B. & O'Doherty, J. P. Reinforcement-learning in fronto-striatal circuits.
803 *Neuropsychopharmacol. 2021 471* **47**, 147–162 (2021).

804 95. Wang, J. X. *et al.* Prefrontal cortex as a meta-reinforcement learning system. *Nat.*
805 *Neurosci.* **21**, 860–868 (2018).

806 96. Lee, D. & Seo, H. Mechanisms of Reinforcement Learning and Decision Making in the
807 Primate Dorsolateral Prefrontal Cortex. *Ann. N. Y. Acad. Sci.* **1104**, 108–122 (2007).

808 97. Sailer, U., Flanagan, J. R. & Johansson, R. S. Eye–Hand Coordination during Learning of
809 a Novel Visuomotor Task. *J. Neurosci.* **25**, 8833–8842 (2005).

810 98. Land, M. F. Eye movements and the control of actions in everyday life. *Prog. Retin. Eye*
811 *Res.* **25**, 296–324 (2006).

812 99. Gerstner, W., Kempter, R., Van Hemmen, J. L. & Wagner, H. A neuronal learning rule
813 for sub-millisecond temporal coding. *Nat. 1996 3836595* **383**, 76–78 (1996).

814 100. Gilson, M., Burkitt, A. & Leo van Hemmen, J. STDP in recurrent neuronal networks.
815 *Front. Comput. Neurosci.* **4**, 23 (2010).

816 101. Gerstner, W., Lehmann, M., Liakoni, V., Corneil, D. & Brea, J. Eligibility Traces and
817 Plasticity on Behavioral Time Scales: Experimental Support of NeoHebbian Three-
818 Factor Learning Rules. *Frontiers in Neural Circuits* **12**, 53 (2018).

819 102. Perrin, E. & Venance, L. Bridging the gap between striatal plasticity and learning.
820 *Current Opinion in Neurobiology* **54**, 104–112 (2019).

821 103. Bittner, K. C., Milstein, A. D., Grienberger, C., Romani, S. & Magee, J. C. Behavioral time
822 scale synaptic plasticity underlies CA1 place fields. *Science (80-.).* **357**, 1033–1036
823 (2017).

824 104. Suvrathan, A. Beyond STDP — towards diverse and functionally relevant plasticity

rules. *Current Opinion in Neurobiology* **54**, 12–19 (2019).

105. Mansvelder, H., Verhoog, M. & Goriounova, N. Synaptic plasticity in human cortical circuits: cellular mechanisms of learning and memory in the human brain? *Curr. Opin. Neurobiol.* **54**, 186–193 (2019).

106. Barbosa, J. *et al.* Interplay between persistent activity and activity-silent dynamics in the prefrontal cortex underlies serial biases in working memory. *Nat. Neurosci. 2020 238* **23**, 1016–1024 (2020).

107. Stokes, M. G. 'Activity-silent' working memory in prefrontal cortex: A dynamic coding framework. *Trends in Cognitive Sciences* **19**, 394–405 (2015).

108. Mongillo, G., Barak, O. & Tsodyks, M. SynaptiC Theory of Working Memory. *Science (80-.).* **319**, 1543–1546 (2008).

109. Lim, DH., Yoon, Y.J., Her, E. et al. Active maintenance of eligibility trace in rodent prefrontal cortex. *Sci Rep 10, 18860* (2020). doi:https://doi.org/10.1038/s41598-020-75820-0

110. Parker, N. F. *et al.* Choice-selective sequences dominate in cortical relative to thalamic inputs to NAc to support reinforcement learning. *Cell Rep.* **39**, 110756 (2022).

111. Harvey, C. D., Coen, P. & Tank, D. W. Choice-specific sequences in parietal cortex during a virtual-navigation decision task. *Nature* (2012). doi:10.1038/nature10918

112. Koay, S. A., Charles, A. S., Thiberge, S. Y., Brody, C. D. & Tank, D. W. Sequential and efficient neural-population coding of complex task information. *Neuron* **110**, 328-349.e11 (2022).

113. Krumin, M., Lee, J. J., Harris, K. D. & Carandini, M. Decision and navigation in mouse parietal cortex. *Elife* (2018). doi:10.7554/eLife.42583

114. Sommer, M. A. & Wurtz, R. H. *Visual perception and corollary discharge*. *Perception* **37**, (2008).

115. Sommer, M. A. & Wurtz, R. H. Brain circuits for the internal monitoring of movements. *Annu. Rev. Neurosci.* **31**, 317 (2008).

116. Xu, B. Y., Karachi, C. & Goldberg, M. E. The Postsaccadic Unreliability of Gain Fields Renders It Unlikely that the Motor System Can Use Them to Calculate Target Position in Space. *Neuron* **76**, 1201–1209 (2012).

117. Land, M. F. & McLeod, P. From eye movements to actions: how batsmen hit the ball. *Nat. Neurosci.* **3**, 1340–1345 (2000).

118. Wurtz, R. H. Corollary Discharge Contributions to Perceptual Continuity Across Saccades. *https://doi.org/10.1146/annurev-vision-102016-061207* **4**, 215–237 (2018).

119. Heinzle, J., Aponte, E. A. & Stephan, K. E. Computational models of eye movements and their application to schizophrenia. *Heinzle, Jakob; Aponte, Eduardo A; Stephan, Klaas E (2016). Comput. Model. eye movements their Appl. to Schizophr. Curr. Opin. Behav. Sci. 1121-29.* **11**, 21–29 (2016).

120. Adámek, P., Langová, V. & Horáček, J. Early-stage visual perception impairment in schizophrenia, bottom-up and back again. *Schizophr. 2022 81* **8**, 1–12 (2022).

121. Broerse, A., Crawford, T. J. & Den Boer, J. A. Parsing cognition in schizophrenia using saccadic eye movements: a selective overview. *Neuropsychologia* **39**, 742–756 (2001).

122. Egaña, J. I. *et al.* Small saccades and image complexity during free viewing of natural images in schizophrenia. *Front. Psychiatry* **4**, 37 (2013).

123. Brody, C. D., Romo, R. & Kepecs, A. Basic mechanisms for graded persistent activity: discrete attractors, continuous attractors, and dynamic representations. *Curr. Opin. Neurobiol.* **13**, 204–211 (2003).

124. Wang, X.-J. Decision making in recurrent neuronal circuits. *Neuron* **60**, 215–34 (2008).

125. Wang, X. J. Synaptic reverberation underlying mnemonic persistent activity. *Trends Neurosci.* **24**, 455–463 (2001).

126. Ganguli, S., Huh, D. & Sompolinsky, H. Memory traces in dynamical systems. *Proc. Natl. Acad. Sci. U. S. A.* **105**, 18970–18975 (2008).

127. Goldman, M. S. Memory without Feedback in a Neural Network. *Neuron* **61**, 621 (2009).

128. Rajan, K., Harvey, C. D. D. & Tank, D. W. W. Recurrent Network Models of Sequence Generation and Memory. *Neuron* **90**, 128–142 (2016).

129. Kaufman, M. T., Churchland, M. M., Ryu, S. I. & Shenoy, K. V. Cortical activity in the null space: permitting preparation without movement. *Nat. Neurosci. 2014 173* **17**, 440–448 (2014).

130. Genovesio, A., Brasted, P. J. & Wise, S. P. Representation of Future and Previous Spatial Goals by Separate Neural Populations in Prefrontal Cortex. *J. Neurosci.* **26**, 7305–7316 (2006).

131. Gnadt, J. W. & Andersen, R. A. Memory related motor planning activity in posterior parietal cortex of macaque. *Exp. brain Res.* **70**, 216–220 (1988).

132. Ding, L. & Gold, J. I. Caudate encodes multiple computations for perceptual decisions. *J. Neurosci.* **30**, 15747–15759 (2010).

Extended Data

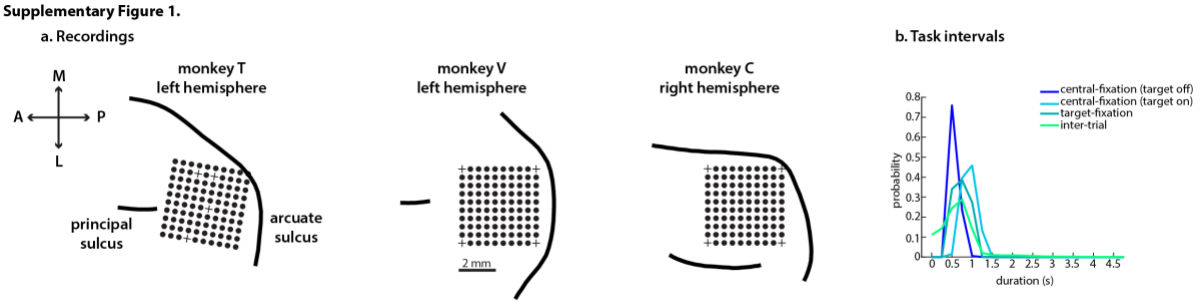

Supplementary Figure 1. ***Recording locations in prefrontal cortex and task***

a. In all three monkeys, we obtained single-unit and multi-unit recordings from a 10x10 array implanted in pre-arcuate cortex. Black circles indicate the cortical locations of the 96 electrodes used for recordings.

b. Durations of four intervals occurring in each trial. Central-fixation (target off): from the onset of the start saccade until the onset of the visual target. Central-fixation (target on): from the onset of the visual target until the offset of the fixation point. Target-fixation: from the onset of the rewarded saccade until the reward delivery. Inter-trial: from the reward delivery of a given trial until the onset of the fixation cross on the next trial.

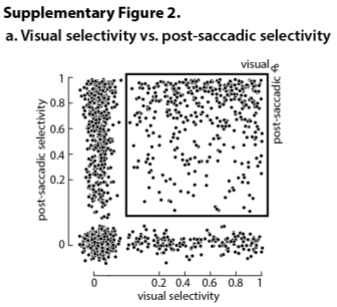

Supplementary Figure 2. ***Visual selectivity vs. post-saccadic selectivity****.*

a. Visual modulation at single-unit level. We find no relation between the selectivity of post-saccadic units at target presentation vs. post-saccadic epoch. This finding suggests that post-saccadic activity cannot be explained by visual responses elicited by the saccade and the resulting appearance of "new" visual features in a unit's receptive field.

Supplementary Figure 3.

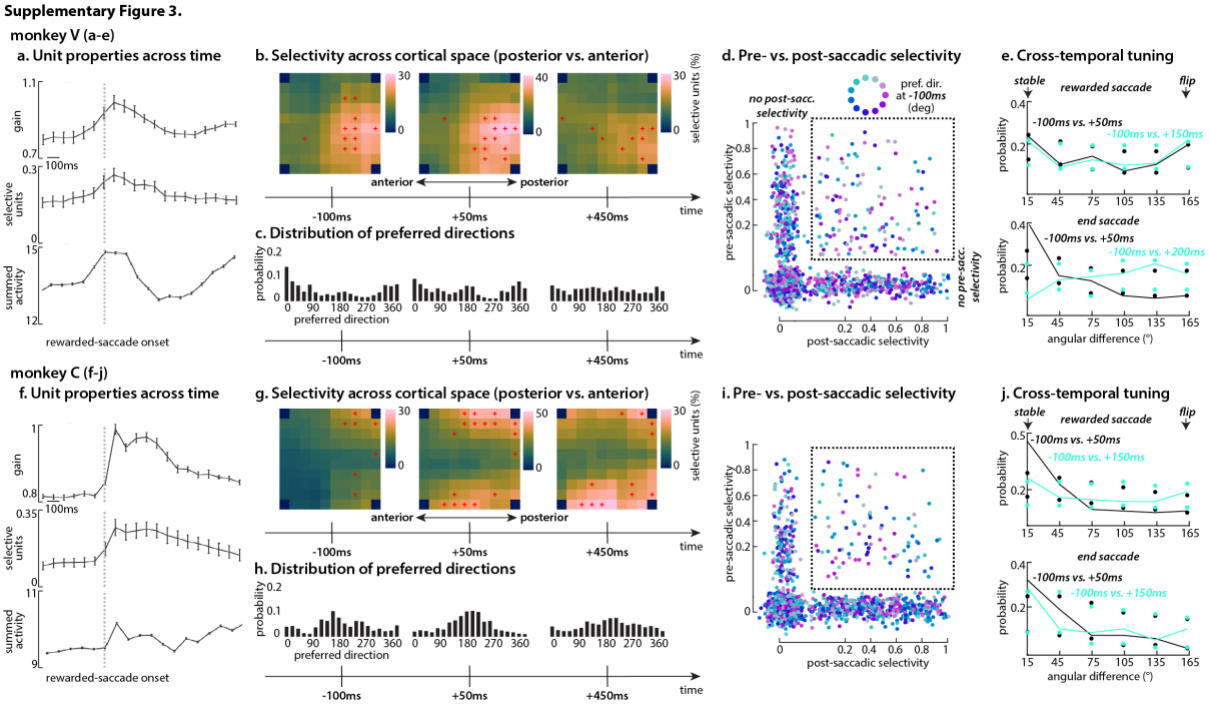

Supplementary Figure 3. ***Dynamics of directional selectivity in single units in monkey V and C.***

Same conventions as in Figure 2 and Figure 4. a-e: monkey V; f-j: monkey C.

a&f. Single-unit properties around the rewarded saccade, analogous to Figure 2.

b&g. Unit selectivity as a function of cortical space.. Similarly to monkey T (Figure 2), selectivity at anterior locations appears to at post-saccadic times. Red crosses indicate values outside the 90% confidence intervals of a shuffled null-distribution assuming no relation between unit selectivity and electrode location.

c&h. Distribution of preferred directions. Similarly to monkey T (Figure 2), pre-saccadic preferred directions are more contralateral (centered at 0° for monkey V and centered at 180° for monkey C), while post-saccadic preferred directions are more evenly distributed. Only selective units are included.

d&i. Pre vs. post-saccadic selectivity. Similarly to monkey T (Figure 4), many units have post-saccadic selectivity, but not pre-saccadic selectivity (close to horizontal axis). However, fewer units show both pre and post-saccadic selectivity compared to monkey T.

e&j. Cross-temporal tuning for the rewarded saccade (top) and the end saccade (bottom) for units with both pre and post-saccadic selectivity (curves, points show 5th and 95th confidence intervals of a shuffle null-hypothesis assuming no relation between pre- and post-saccadic preferred directions). As in monkey T (Figure 4), the preferred direction tends to "flip" between the pre and post-saccadic epochs for the rewarded saccade in monkey V (e, top; curves at 180° outside the confidence intervals) but for neither saccade in monkey C (j; curves at 180° inside the confidence intervals). However, pre-saccadic tuning is weak in monkey C (i), making a comparison of pre and post-saccadic tuning challenging.

Supplementary Figure 4.

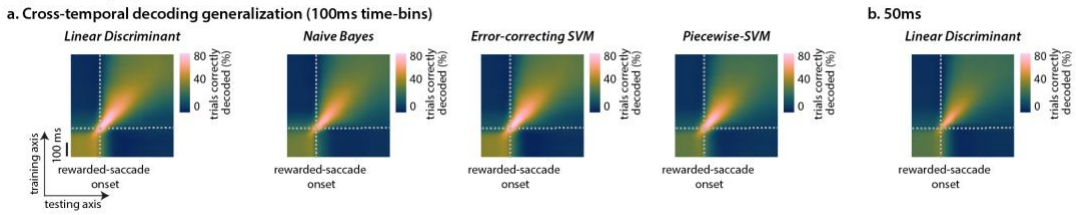

Supplementary Figure 4. ***Decoding of the rewarded-saccade for different decoders and binning****.*

a. Cross-temporal decoding matrix (as in Figure 3b) for different choices of decoders (titles).

b. Cross-temporal decoding matrix for shorter temporal bins, of 50ms instead of 100ms as in a. Decoding is performed with linear discriminant analysis, as in a, left.

The structure of the decoding matrices, and in particular the signatures of a dynamic representation of direction during the post-saccadic epoch, are robust to the choice of decoder and bin duration.

Supplementary Figure 5.

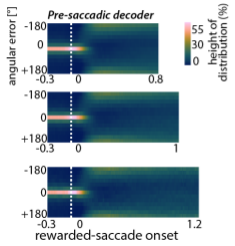

Supplementary Figure 5. ***Read-out flips from pre-saccadic decoders persists throughout the target-fixation period.***

We applied a pre-saccadic decoder to activity before and after the rewarded saccade (as in Figure 3c, pre-saccadic decoder). We separated trials based on the duration of the target-fixation period (0.8s, 1s and 1.2s). In particular for rewarded saccades to contralateral angles, the flip in read-out following the saccade (angular errors close to 180 degrees) persists largely unchanged until the end of even the longest target-fixation periods.

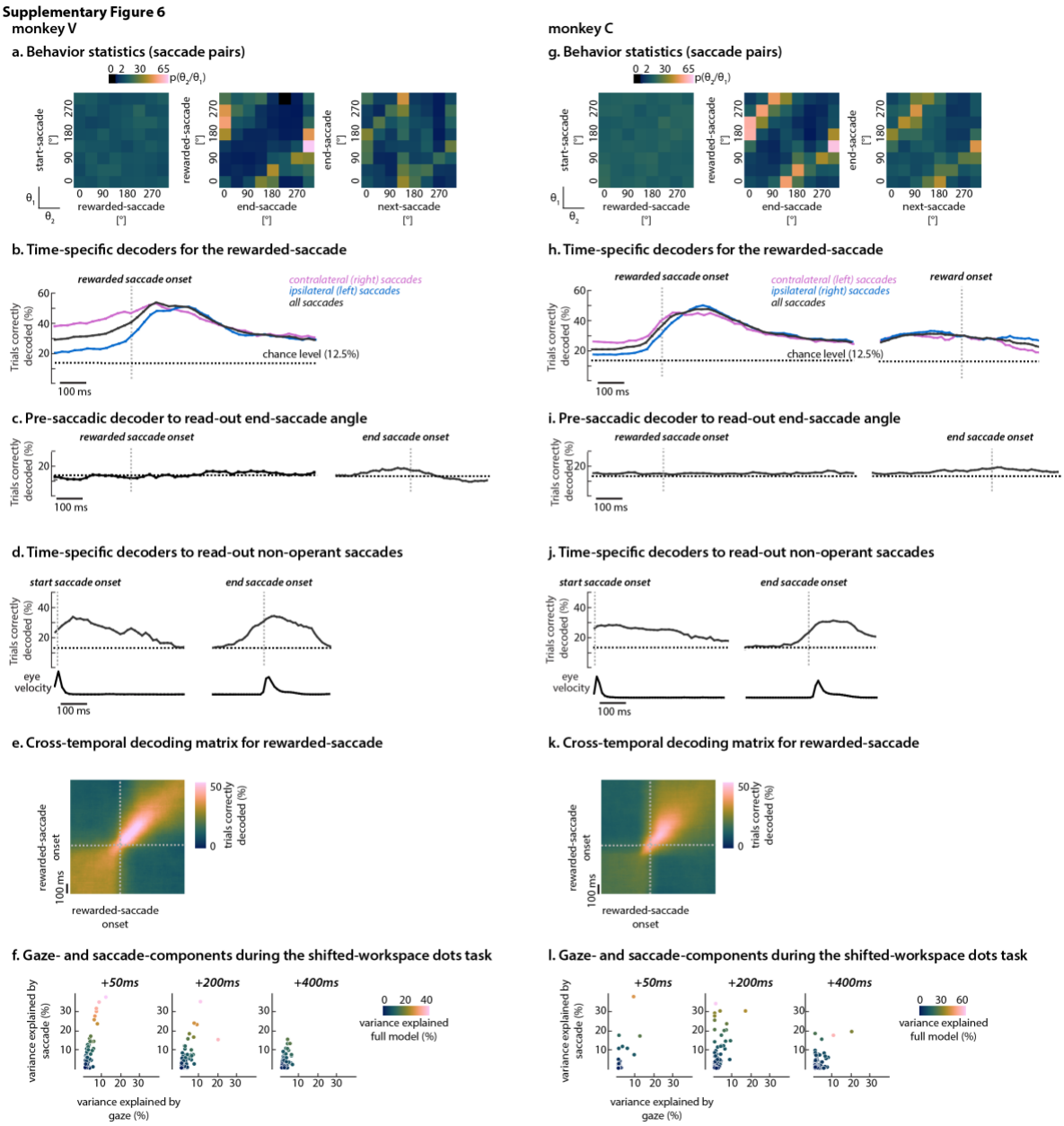

Supplementary Figure 6. ***Main properties of population-level saccade representations in monkeys V and C.***

a-f: Data for monkey V.

a. Statistics of subsequent saccades, analogous to Figure 5b.

b. Time-specific decoding of the direction of the rewarded saccade, as in Figure 3a.

c. Decoding the direction of the end saccade, based on a pre-saccadic decoder trained on rewarded saccades. Analogous to Figure 5c.

d. Time-specific decoding of the direction of the start and end saccades, based on corresponding decoders trained on rewarded saccades. Analogous to Figure 5a.

e. Cross-temporal decoding matrix for the rewarded saccade. Analogous to Figure 3b.

f. Modulation of single unit activity by gaze and direction components in the shifted work-space dots task. Analogous to Figure 6b.

h-l: Analogous to a-f, but data from monkey C.

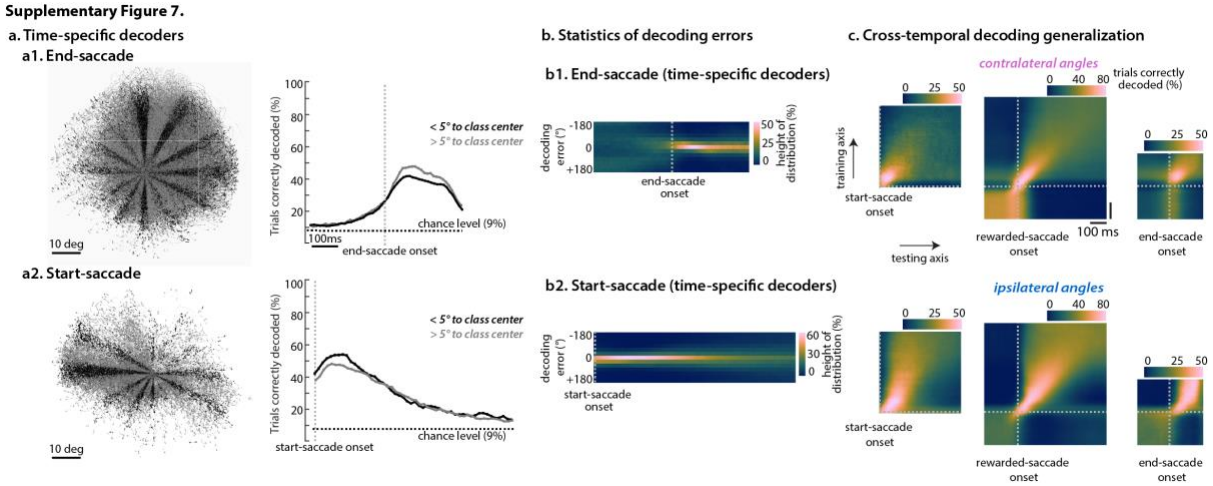

Supplementary Figure 7. ***Population-level representations of end and start saccades in monkey T.***

a. Saccade end points (left) and time-specific decoding (right) for end (top) and start saccades (bottom). Unlike for the rewarded saccades, the direction of the end and start saccades is continuous. We can apply the decoders trained on the rewarded saccade if we bin this continuous value into bins whose centers are the directions of the rewarded saccade. To study how this binning affects the decoding performance, we assigned saccades into two groups: saccades with directions close to the respective category center (left, black; resulting in a distribution of directions similar to that for the rewarded saccade; as in Figure 1b, center - eye trajectories of the rewarded saccade) and saccades with directions far from this center (gray). Decoding performance for both groups is similar to performance when all trials are included Figure 5a. The lower decoding performance of end and start saccades compared to rewarded saccades thus is not a consequence of the different distribution of saccade directions.

b. The distribution of angular errors for the end and start saccades, analogous to Figure 3c. Same decoders as in a.

c. Cross-temporal decoding matrix for the end (left) and start saccades (right), compared to that for the rewarded saccade (middle; replotted from Figure 3b), separately by saccade laterality (top vs. bottom). Same decoders as in a, but here applied also to time-points outside their training time-window. The structure of the decoding matrices, and in particular the signatures of a dynamic representation of direction during the post-saccadic epoch, are preserved across different saccade types.

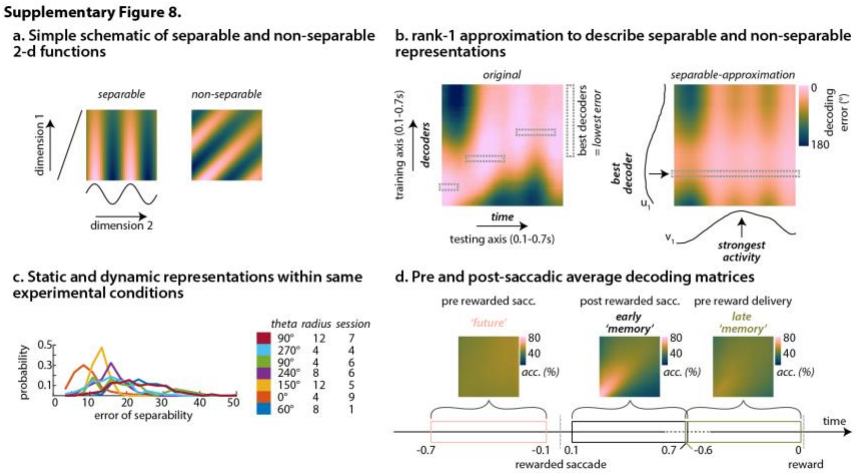

Supplementary Figure 8. ***Time stability of saccade representation on single trials: definition and examples.***

a. Schematic of separable and non-separable 2-d functions. Separable functions can be written as the product of two functions.

b. Example single-trial decoding matrix. Decoders are trained at a specific time (vertical axis) and evaluated at another time (horizontal axis) on responses from a single trial. Color indicates decoding error (i.e. an angle). We approximate each measured decoding matrix (left) with its best separable approximation (right). In the approximation, each value of the matrix is expressed as the product of two functions - u_1 (capturing the overall performance of each decoder) and v_1 (capturing the overall strength of saccadic responses at each time). The original matrix reveals dynamic coding: no single decoder outperforms all others across all post-saccadic times. The separable approximation cannot capture this structure: by construction, a single decoder (i.e. location along the vertical axis) leads to optimal decoding (smallest errors) at all times (horizontal axis).

c. Each example contains the distribution of error-of-separability values within the same condition. A condition is defined by the recording session and the rewarded saccade parameters, i.e. direction and radius.

d. Average decoding matrices for the direction of the rewarded saccade, at three times in the trial: before onset of the rewarded saccade, right after the saccade, and before the reward delivery. Analogous to Figure 3b, computed using decoding accuracy (0 or 1). Pre-saccadic activity appears to be stable on average ('future'), while post-saccadic activity appears to be dynamic - more so early on ('early memory') than late after saccade execution ('late memory').

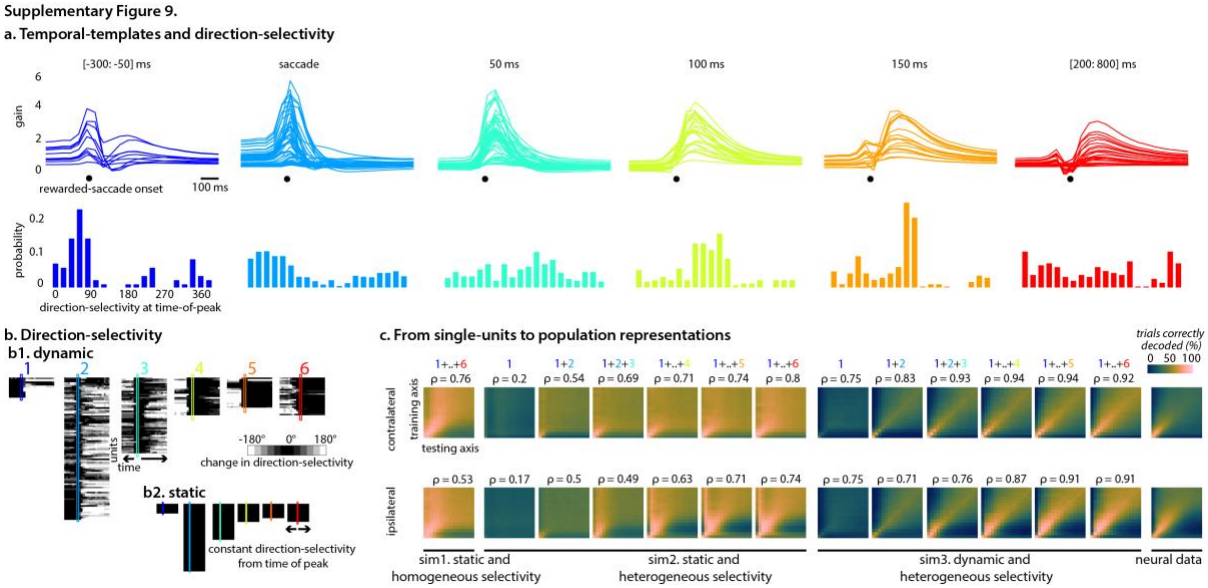

Supplementary Figure 9. ***Relation of post-saccadic representations at the single unit and population levels****.*

a. Unit-specific temporal-templates. Gain is one of the three free parameters of the unimodal model of time-specific direction-averaged responses. For each unit,, we assemble all the time-specific, estimated gains and build a unit-specific temporal-template. Direction-averaged responses are z-scored (across time and conditions) prior to model fitting, and thus, the gain indicates the unit's response at its preferred direction as number of standard-deviations from its mean response. The unit-specific estimated gains are de-noised by projecting onto the first 3 PCs (90% variance). In the upper panel, each line represents a unit and units are sorted into groups based on the time-of-peak in the estimated gain. The lower panel contains the distribution of direction-selectivity at the time-of-peak for each unit in the respective group.

b. Direction-selectivity. b1. Empirical: Change in direction-selectivity relative to the optimal direction at the time-of-peak for each unit in the respective group (1 – peak at 50ms, 2 – peak at 100ms, 3 – peak at 150ms, 4 – peak during [200: 800]ms). b2. Simulation: No change in direction-selectivity, i.e. the direction-selectivity at the time-of-peak is sustained.

c. Three simulations using Poisson neurons with temporal-templates like the ones estimated in a. ***Simulation 1****: static direction-selectivity (b2) and homogeneous selectivity (The distribution of direction-selectivity at time-of-peak is uniform for each group of units).* ***Simulation 2****: static direction-selectivity (b2) and heterogeneous selectivity (Empirical distribution of direction-selectivity at time-of-peak – lower panel in a). Decoding matrices are obtained by progressively adding groups of neurons (for e.g. 1+2 refers to units from group 1 and group 2).* ***Simulation 3****: dynamic direction-selectivity (b1) and heterogeneous selectivity. Last column displays the decoding matrix computed from the neural data. Linear correlation ρ between decoding matrices computed from simulated responses and the empirical decoding matrix. Simulation 3 best captures the structure of the empirical decoding matrix for both ipsilateral (left) and contralateral (right) saccades.*

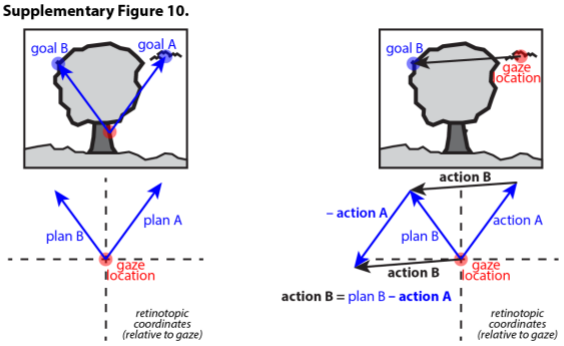

Supplementary Figure 10. ***Vector subtraction mechanism for spatially accurate saccades.***

Diagram suggesting how a vector subtraction mechanism could be used to adjust sensory representations across saccades. Suppose the motor plan is to perform two consecutive saccades to two targets, goal A and goal B. Left panel: The motor plan is constructed while the gaze is at the bottom of the tree (red circle) and uses the retinal registration of the two targets, plan A and plan B. Right panel: The first saccade (action A) corresponds to plan A, and is thus a consonant-vector saccade. The second saccade is, on the other hand, a dissonant-vector saccade, because the movement vector does not correspond to the original retinal registration plan B. The movement-vector of the second saccade (action B) is obtained by subtracting the vector of the intervening (first) saccade from the retinal registration of the second target: action B = plan B - action A. See Fig. 13 in [45].

Primate pre-arcuate cortex actively maintains persistent representations of saccades from plans to outcomes

Methods description

Table of Contents

Experimental procedures

We collected behavioral and neural data from three adult male rhesus monkeys: monkeys T (14 kg), V (11 kg) and C. All surgical, behavioral, and animal-care procedures complied with National Institutes of Health guidelines and were approved by the Stanford University Institutional Animal Care and Use Committee. Prior to training, the monkeys were implanted

with a stainless-steel head holder[1] and a scleral search coil for monitoring monocular eye position[2]. We used operant conditioning with liquid rewards to train the monkeys to perform a visually guided, delayed-saccade task and a two-alternative, forced-choice, motion discrimination task.

During training and experimental sessions, monkeys sat in a primate chair with their head restrained. Visual stimuli were presented on a cathode ray tube monitor controlled by a VSG graphics card (Cambridge Graphics, UK), at a frame rate of 120Hz, and viewed from a distance of 57 cm. Eye movements were monitored through the scleral eye coils (C-N-C Engineering, Seattle, WA). Behavioral control and data acquisition were managed by a computer running the REX software environment and QNX Software System's (Ottawa, Canada) real-time operating system.

Behavioral tasks

Instructed saccade task

Monkeys were engaged in a visually-guided, delayed-saccade task, requiring them to perform a sequence of saccades and fixations on each trial to obtain a reward (Fig. 1a). A trial was initiated by a saccade to the fixation point, and subsequently the monkey was required to maintain fixation until the offset of the fixation point. At 0.6-0.8s after fixation onset, a saccade target was presented in the periphery (33 unique positions per experiment for monkey T). The fixation cue disappeared after an interval of random duration following the target onset (0.7-1.2s) instructing the monkey to execute the saccade to the target. After the saccade, the monkey was again required to maintain fixation, this time on the target, for the duration of another random time interval (0.8-1.5s). At the end of this interval, the target disappeared, a reward was delivered, and the monkey was free to move the eyes.

Note that for monkey T possible targets were place 30 degrees apart, but only 11 out of 12 ({0, 30, 60, 90, 120, 150, 180, 210, 240, 270, 300, 330} degrees) directions were used per experiment. Specifically, targets at 120 degrees were never present in 5 sessions; 300 degrees in 3 sessions and 210 degrees in one session. The presented targets could appear in one of three radii (4, 8, 12). Therefore, chance level of decoding analyses is computed using 11 classes (0.09). For monkey V and monkey C, each recording session included 24 unique target locations (8 target directions placed at 45 degrees apart and 3 possible radii - 4, 8 and 12).

Perceptual decision-making task (moving-dots)

Monkeys were engaged in a two-alternative, forced-choice perceptual discrimination task. The timing of task events was similar to the instructed saccade task (included the random interval of target-fixation after choice saccade), but here the monkeys had to choose between two targets based on the dominant direction of motion in a cloud of random-dots stimulus. Correct choices (e.g. a saccade to the right target for predominant rightward motion) were rewarded at the end of the target-fixation-period. The strength of the motion stimulus

(motion coherence) was set pseudo-randomly on each trial. For low motion coherences, the monkeys' performance was close to chance level (50%), while for high coherences it was close to perfect.

Shifted workspace for the perceptual task

We used a modified version of the moving-dots task to investigate whether post-saccadic activity of the rewarded saccade is affected by the position of the eye. The timing of relevant task-events was analogous to that in the instructed saccade task, and included a target-fixation-period after the rewarded saccade (i.e. the choice saccade). Critically, each experiment in this task included trials from two "shifted" workspaces, whereby the location of the fixation point was shifted to the left from the midline in one workspace (relative to head-position), and to the right in the other (Fig. 6a, "left" and "right" workspaces). As a result, saccade direction and gaze-location of the rewarded saccade are somewhat decoupled—for example, the location corresponding to the center of the monitor could either be the target of a rightward or a leftward saccade (Fig. 6a, left vs. right workspace).

Same recording day for perceptual task and instructed saccade task with 2 targets

On some recording days, monkeys performed two tasks sequentially: the perceptual task (random-dots), followed by the instructed saccade task with two targets. Importantly, the target locations across the two tasks were identical, allowing the comparison of pre and post-saccadic activity across the two tasks.

Neural recordings

We recorded single and multi-unit neural signals with a chronically-implanted 10 by 10 array of electrodes (Cyberkinetics Neurotechnology Systems, Foxborough, MA; now Blackrock Microsystems). The inter-electrode spacing was 0.4 mm; electrodes were 1.5 mm long. Arrays were surgically implanted into the pre-arcuate gyrus[3,4]. We targeted the array to a region of prefrontal cortex between the posterior end of the principal sulcus, and the anterior bank of the arcuate sulcus, near the rostral zone of Brodmann's area 8 (area 8Ar) in monkeys T and V. The arrays were implanted in the left hemisphere in both monkeys. The exact location of the array varied slightly across the two monkeys (Supplementary Figure 1a), due to inter-animal variations in cortical vasculature and sulcal geometry that constrained the location of the array insertion site. In monkey C the array was placed between the superior branch of arcuate sulcus and dorsal bank of the principal sulcus, in the right hemisphere.

Array signals were amplified with respect to a common subdural ground, filtered and digitized using hardware and software from Cyberkinetics. For each of the 96 recording channels,

'spikes' from the entire duration of a recording session were sorted and clustered offline, based on a principal component analysis of voltage waveforms, using Plexon Offline Sorter (Plexon Inc., Dallas, Texas). This automated process returned a set of candidate action-potential classifications for each electrode that were subject to additional quality controls, including considerations of waveform shape, waveform reproducibility, inter-spike interval statistics, and the overall firing rate. For clusters returned by this post-processing, both spike-waveform and spike-timing metrics fell within previously-reported ranges for array recordings[3].

Daily recordings yielded ~100-200 single and multi-unit clusters distributed across the array. We do not differentiate between single-unit and multi-unit recordings, referring to both collectively as 'units'. Therefore, we also do not draw conclusions in this study that depend on the distinction between single and multi-unit responses. Neural responses in the instructed saccade task were recorded over a total of 9, 10, 10 experiments in monkeys monkey T, monkey V and monkey C, for a total of 20,905, 4751 and 8611 trials.

Analysis of eye movement data

Saccade extraction

We used a non-parametric data-driven method for classifying eye fixations and saccades that automatically adapts itself to the task statistics[5]. The method is built on the assumption that the eye reaches higher speeds during saccades than during fixations, and that there are fewer peaks in speed due to saccades than due to fixations. Using these observations about the statistics of eye-behavior, the methods derives an optimum speed threshold that best separates the speed distribution of saccades from the speed distribution of fixations and instrumental noise.

Saccade types

We analyze neural activity related to different types of saccades, i.e. the instructed and freely initiated saccades occurring before, during, and after each trial. We refer to the initial saccade to the fixation point as the *start saccade*, the saccade to the target as the *rewarded saccade*, and the saccade away from the target after reward delivery as the *end saccade*. The start saccade is therefore visually-guided and non-rewarded; the rewarded saccade is visually-guided and rewarded; and the end saccade is free and non-rewarded. Monkeys initiate the end saccade when there is nothing on the screen. The saccade durations are 30+-30ms, 40+-10ms and 140+-80ms, for the start, rewarded and end saccades respectively.

Analysis of neurophysiology data

Throughout the paper, we consider neural responses occurring during four distinct, largely non-overlapping trial epochs. We refer to the first randomized time interval, following the start saccade, as the *first central-fixation-period* (i.e. fixation on the fixation point, 0.6-0.8s); the second randomized interval, preceding the rewarded saccade, as the *second central-fixation-period* (0.7-1.2s); and the last randomized interval, preceding the reward, as the *target-fixation-period* (i.e. fixation on the target, 0.8-1.5s). The fourth epoch is centered around the end saccade, whose onset is after reward delivery. Notably, the onset of the end saccade does no coincide with the time of reward delivery on every single trial - on some trials monkeys initiate the end-saccade immediately after reward and on some trials monkeys continue fixating the location where the target was present, on a few trials for intervals as long as 600ms (see Fig. 3a).

Unit-specific direction selectivity

Pre-processing condition-averaged responses

We normalized the unit responses using z-scoring:

$$z_{i,t}(l) = \frac{z_{i,t}^{\mathrm{raw}}(l) - \langle z_{i,t}^{\mathrm{raw}}(l) \rangle_{t,l}}{std(z_{i,t}^{\mathrm{raw}}(l))_{t,l} + \bar{\sigma}}$$

where $z_{i,t}^{\mathrm{raw}}(l)$ and $z_{i,t}(l)$ are the raw firing rate and z-scored responses, respectively, of unit *i* at time *t* and on trial *l*, $\langle \cdot \rangle_{t,l}$ and $std_{t,l}$ indicate the mean and standard deviation across times and trials, and $\bar{\sigma}$ is a constant defined as the median of the standard deviation across all units in a session.

We defined condition-averaged responses $f_{i,t,c}$ for each unit by averaging the normalized time-varying firing rates across all trials belonging to a given condition $'c'$. For the instructed saccade task, we define each condition by the saccade direction (11 conditions for monkey T, 8 conditions for monkey V and monkey C).

The condition-averaged responses were de-noised using Singular Vector Decomposition (SVD). We concatenated the condition-averaged responses $f_{i,t,\theta}$ across all recording sessions with the same conditions in a $N_{unit} \times (N_{condition} \cdot T)$ matrix, where N_{unit} is the total number of units, $N_{condition}$ is the total number of conditions, and *T* is the number of bins. The left singular-vectors of this data matrix are vectors $\boldsymbol{v}_a$ of length N_{unit}, indexed by a, ordered from the singular-vector explaining the most variance to the one explaining the least. We use the first N_{svd} singular-vectors to define a de-noising matrix $\boldsymbol{D}$ of size $N_{unit} \times N_{unit}$:

$$\boldsymbol{D} = \sum_{a=1}^{N_{svd}} \boldsymbol{v}_a \boldsymbol{v}_a^T$$

We used this matrix to de-noise the condition-averaged responses by projecting them into the sub-space spanned by the first N_{svd} singular-vectors:

$$f_{i,t,\theta}^{svd} = \boldsymbol{D} f_{i,t,\theta}$$

We use the de-noised condition-averaged responses $f_{i,t,\theta}^{svd}$ to determine the unit-specific optimal direction, i.e. the condition that elicits the highest responses. From now on $f_{i,t,\theta}$ will refer to the de-noised responses.

Gaussian Fits for condition-averaged responses

We estimated, for each unit, the saccade-location that elicits the highest response at each time by fitting a descriptive function[6] to the normalized time-varying condition-averaged responses:

$$g(\theta) = baseline_\theta + gain_\theta * \exp\left(-\frac{(\theta - \theta_0)^2}{2\sigma_\theta^2}\right)$$

where θ_0 is the preferred saccade direction, σ_θ determines the tuning width and $gain_\theta$ determines the modulation depth of the tuning curve.

We fitted the parameters of these models separately for each unit to averaged responses grouped by saccade-direction within the epoch [-0.3, 0.5]s around saccade initiation, in 50ms non-overlapping bins. The models are fit by minimizing the summed square error across the respective conditions between the model predictions and the corresponding condition-averaged response.

Goodness-of-fit

We validated the 1-D Gaussian models by computing a coefficient of determination (R^2) value from the measured condition-averaged response $f_{i,t,\theta}$ and the model's reconstruction $\widehat{f_{i,t,\theta}}$, based on comparing the variability of the estimation errors with the variability of the original neural responses.

$$r_{i,t,\theta}^2 = \max\left(0, 1 - \frac{\sum_\theta ||f_{i,t,\theta} - \widehat{f_{i,t,\theta}}||^2}{\sum_\theta (f_{i,t,\theta} - \langle f_{i,t,\theta} \rangle_\theta)^2}\right)$$

Model parameters were found from condition-averages computed on a subset of trials (training set) and validated on condition-averages computed on a different, non-overlapping subset of trials (testing set). All units that had a coefficient of determination different than 0 were considered selective. A coefficient of determination equal to 0 indicates that the condition-averaged response is better described by the averaged response across all conditions $\langle f_{i,t,\theta} \rangle_\theta$.

Cross-temporal selectivity matrices

We quantified the percentage of selective units at different time-pairs (t_m, t_n):

$$n_{(t_m, t_n)} = \sum_k \begin{cases} 1; & \text{if } r^2_{i,t_m,\theta} > 0 \text{ and } r^2_{i,t_n,\theta} > 0 \\ 0; & \text{otherwise} \end{cases}$$

where i is unit index.

To assess the significance of each $n_{(t_m, t_n)}$, we shuffled the unit-order independently at t_m and t_n and re-computed the number of units that were selective at both times. We repeated this procedure 1000 times and compared the measured $n_{(t_m, t_n)}$ to the 95th percentile of this distribution.

Poisson simulations

We simulate Poisson spike trains (Supp. Fig. 9) for the time interval [-300, 800]ms around the rewarded-saccade. This total interval of 1100ms is divided into 22 non-overlapping bins of 50ms each. The average firing rate in each bin is $r_i(t)$ where i is unit-id and t is a 50ms bin.

First, we subdivide each bin into 50 sub-bins of $\delta t = 1ms$ indexed by k. Then we generate a sequence of random numbers $x[k]$, uniformly distributed between 0 and 1. For each sub-bin k, if $x[k] \leq r\delta t$ ($r(t)$ is constant within each bin), we generate a spike, otherwise, if $x[k] > r\delta t$, there is no spike.

The underlying firing rate in each bin is given by the condition-averaged response (previously noted as $f_{i,t,\theta}$):

$$r_i(t) = baseline + ct * gain_{\theta,i} * \exp\left(-\frac{(\theta - \theta_{0,i,t})^2}{2\sigma_\theta^2}\right)$$

where $baseline = 5, \sigma_\theta^2 = 45°, gain_{\theta,i}$ is estimated from the neural data, $ct = 15$ is chosen such that the average firing rate of the simulations to match the recorded average firing rates (Fig. 7b). We consider different distributions and dynamics for $\theta_{0,i,t}$. In Simulation 1 (static and homogeneous selectivity) $\theta_{0,i,t}$ is uniformly distributed and does not change across time

– in other words, all saccade directions are equally well represented at all times. In Simulation 2 (static and heterogeneous selectivity) the distribution of $\theta_{0,i,t}$ matches the empirical distribution at the time-of-peak, i.e. for each neuron we 'freeze' the preferred direction it has when it reaches peak selectivity during the interval [-0.3, 0.8]s, and impose that it keeps this preferred direction across the entire interval. Simulation 3 matches the real case (dynamic and heterogeneous selectivity), where the distribution of $\theta_{0,i,t}$ matches the moment-to-moment empirical distribution of preferred directions.

Population Decoding

We quantified the relation between single-trial normalized population responses and the saccade direction using high-dimensional decoders suited for multi-class problems. To ensure our results do not depend on the choice of the decoder, we used several types of decoders. Specifically, we used both MATLAB built-in classifiers: Linear discriminant analysis (fitcdiscr), Naive Bayes (fitcnb) and Error-correcting SVM (fitcecoc), as well as a customized classifier (Circular-SVM).

The Circular-SVM was proposed by Graf et al.[7] and builds on the Naïve Bayes model. Knowing that the topography of the neural responses is circular, it learns the pooling weight W in a model-free way, directly from the neural data. We describe the method briefly, for more details see[7].

Discrimination between two saccade directions θ_1 and θ_2 is done using the sign of the Support-Vector Machine (SVM) decision function:

$$y(\theta_1, \theta_2) = \sum_{i=1}^{N_{unit}} w_i(\theta_1, \theta_2) x_i + b(\theta_1, \theta_2) \equiv \log LR(\theta_1, \theta_2)$$

$$\log LR(\theta_1, \theta_2)$$

$$= \log \frac{L(\theta_1)}{L(\theta_2)} = \log L(\theta_1) - \log\ L(\theta_2)$$

$$= \sum_{i=1}^{N_{unit}} [W_i(\theta_1) - W_i(\theta_2)] r_i + [B(\theta_1) - B(\theta_2)] = \sum_{i=1}^{N_{unit}} w_i(\theta_1, \theta_2) x_i + b(\theta_1, \theta_2)$$

The SVM decision function is used as a local linear approximation of the difference between the log-likelihood evaluated at two saccade directions. The entire log-likelihood function is reconstructed by computing the cumulative sum of the empirical log-likelihood ratios of adjacent directions:

$$logL(\theta_j) = \sum_{k=2}^{j} logLR(\theta_k, \theta_{k-1}) = \sum_{i=1}^{N_{unit}} W_i(\theta_j) r_j + B(\theta_j)$$

with $\log(\theta_1) = 0$.

Some pairs of neighboring directions are better separated than others. We modified the original version of the method such that the discriminability of a saccade-direction would only depend on how well it is separated from its two immediate neighboring directions, and not on how well separated are any other two neighboring directions. To compute an unbiased log-likelihood, each angle θ_i takes turn in being the reference ($\log(\theta_i) = 0$). In this manner, we average out the cumulated-error.

Decoding saccade direction of the start, rewarded and end saccades

Rewarded saccade: We study the relationship between the population responses and the rewarded saccade direction through cross-validated high-dimensional decoders.

Start and end saccade: We apply the same decoders we identified for the rewarded saccade to responses aligned to the start and end saccade. Training a new set of decoders on responses aligned to the end saccade resulted on similar cross-validated accuracies when used to read-out the end saccade (results not shown).

Time-specific decoding

Decoders are trained and tested on time-specific responses using 10-fold cross-validation.

Cross-temporal decoding

Decoders are tested on responses outside their training time-window. A decoding matrix $T \times T$ contains the cross-validated decoding accuracy of T time-specific decoders tested on T time-specific population-responses. The diagonal of this decoding matrix is the time-specific decoding accuracy. All decoders are cross-validated, i.e. that even though the decoders are trained at one time and tested at another time, there is no overlap between the train and test trials. This analysis shows how each of the time-specific mappings generalize across responses at other times in the trial.

Post-saccadic activity is not preparatory activity for the next saccade

One possible interpretation of post-saccadic activity is that it encodes the planning of the next saccade. To test this hypothesis, we decoded the direction of the end saccade from the activity during the target-fixation-period.

The biased behaviour of the monkeys (to make 'return' saccades to the fixation point after reward delivery), together with the relationship between pre-saccadic and post-saccadic tuning (the existence of flip tuning (unit-level) Figure 4c and flip read-out (population-level) Figure 3c) is a serious impediment for testing this hypothesis.

Similarly to the cross-temporal decoding matrices, we tested a decoder outside its training time window. Specifically, we used a decoder trained to decode the rewarded-saccade during the pre-saccadic epoch ($t{:}\,t+\Delta t$, where $t=-150ms$ and $\Delta t=50ms$) to decode the saccade direction across the target-fixation and up until the onset of the end-saccade. However, here the decoding procedure differs in two important ways. For one, we use the decoder to read out the direction of the end saccade, not of the rewarded saccade. For another, we evaluate the accuracy of the read-outs separately for trials from a single direction of the rewarded saccade. If we would evaluate trials from all directions at once, and ignore the behaviour statistics (Figure 5c, middle matrix), applying the pre-saccadic read-out to the activity during the target fixation period would give ***above*** chance-level predictions when reading the direction of the end-saccade.

Figure 5e shows that post-saccadic activity following the rewarded saccade does not contain preparatory activity for the end saccade, when these behavioural correlations are 'subtracted' (see histogram of balanced conditions in Figure 5d), but does contain information about the rewarded saccade. Importantly, the decoding accuracies are computed from the same trials in both cases. Note that it is still possible that preparatory activity of the end saccade would exist along another read-out, one that is different from the pre-saccadic read-out of the rewarded saccade. However, we do not have the statistical power to identify a new pre-saccadic read-out for the end-saccade. Nonetheless, this result shows that the inverted tuning of pre-saccadic activity after saccade execution is not a consequence of the next saccade the monkey will perform.

Post-saccadic activity is modulated by task demands

On some recording days monkeys performed two tasks sequentially. One task was the perceptual decision-making task, where the monkeys had to choose between two targets based on sensory information, and the other task was an instructed, delayed saccade-task, where only one peripheral target was presented on each trial. The instructed saccade-task is the same task that we analyzed so far, with the only difference that the peripheral target can appear in only two locations, and importantly, these two locations coincide with the locations of the two targets used in the perceptual task.

We analyzed the responses during the late central-fixation period (300ms prior to saccade execution) and target-fixation period (up to reward delivery). We identified time-dependent directions in state-space that best separate the population responses due to monkey's choices (leftward or rightward) across the two tasks. The direction of the saccade can be

decoded with high accuracy before, during and after saccade execution. Critically, a single set of decoders can be used to read out saccade direction in both tasks, indicating that the time-dependent saccade-related representations do not drastically differ in the two scenarios.

Note that because trials within the two tasks are not intermingled, but come in two sequential blocks, we corrected the single-trial spike counts of any potential population-level drift in the baseline firing rates:

$$\tilde{x}_{i,t,\mathrm{task-1}} = x_{i,t,task-1} - \langle x_{i,t} \rangle_{task-1}$$

$$\tilde{x}_{i,t,\mathrm{task-2}} = x_{i,t,task-2} - \langle x_{i,t} \rangle_{task-2}$$

The decoding analyses was performed on the normalized responses.

Post-saccadic activity does not encode the momentary gaze location

We addressed the question whether post-saccadic activity is better explained by saccade-covariates or eye-position-covariates in a modified version of the perceptual decision-making task, in which the monkeys were presented with two workspace configurations in a blocked design. The task required the monkeys to discriminate the dominant movement of moving dots, and while the two workspaces were retinotopically identical, they were horizontally (or vertically) shifted along the monkey's line of sight, such that the physical location of one target (T1) in one block was identical to the physical location of the other target (T2) in the other block.

$$x_{i,t}(k) = \beta_{0,i,t} + \beta_{\mathrm{choice},i,t}\mathrm{choice}(k) + \beta_{\mathrm{gaze},i,t}\mathrm{gaze}(k) + \beta_{\mathrm{gaze_{abs}},i,t}\mathrm{gaze_{abs}}(k)$$

where $x_{i,t}(k)$ is the z-scored response of unit i at time t and on trial k, $\mathrm{choice}(k)$ is the monkey's choice on trial k (+1 for choice 1 and -1 for choice 2), $\mathrm{gaze}(k)$ is the target-location on trial k (for two sessions the workspace is shifted along the horizontal axis $\mathrm{gaze} = \mathrm{gaze}_x = \{-1; 0; 1\}$ and $\mathrm{gaze}_y = 0$; and for two sessions the workspace is shifted along the vertical axis $\mathrm{gaze}_x = 0$ and $\mathrm{gaze} = \mathrm{gaze}_y = \{-1; 0; 1\}$), $\mathrm{gaze_{abs}}(k)$ is the absolute value of $\mathrm{gaze}(k)$. We introduced $\mathrm{gaze_{abs}}(k)$ to capture a potential non-linear relation between neural responses and gaze. We focused on three time points in the post-saccadic epoch: early (+50ms), middle (+200ms) and late (+400ms).

Because trials within the two retinotopically-identical sessions ($\mathrm{workspace}_1$ and $\mathrm{workspace}_2$) are not intermingled, but come in sequential blocks, we corrected the single-trial spike counts of any potential population-level drift in the baseline firing rates:

$$\tilde{x}_{i,t,\mathrm{workspace}_1} = x_{i,t,\mathrm{workspace}_1} - \langle x_{i,t} \rangle_{\mathrm{workspace}_1}$$

$$\tilde{x}_{i,t,\mathrm{workspace}_2} = x_{i,t,\mathrm{workspace}_2} - \langle x_{i,t} \rangle_{\mathrm{workspace}_2}$$

We identified the regression coefficients $\beta_{\text{choice},i,t}$, $\beta_{\text{gaze},i,t}$, $\beta_{\text{gaze}_{\text{abs}},i,t}$ through 10-fold cross-validation for each unit separately. We next quantified the saccade-related and gaze-related contributions of each unit through a measure of variance explained on the test trials:

$$\text{variance explained}_{i,t,\text{gaze}} = 1 - \frac{\sum_k \left\| \tilde{x}_{i,t} - \hat{x}_{i,t,\text{gaze}} \right\|^2}{\sum_k (\tilde{x}_{i,t} - \langle \tilde{x}_{i,t} \rangle_k)^2}$$

where

$$\hat{x}_{i,t,\text{gaze}}(k) = \beta_{0,i,t} + \beta_{\text{gaze},i,t}\text{gaze}(k) + \beta_{\text{gaze}_{\text{abs}},i,t}\text{gaze}_{\text{abs}}(k)$$

Similarly for saccade-related activity:

$$\text{variance explained}_{i,t,\text{saccade}} = 1 - \frac{\sum_k \left\| \tilde{x}_{i,t} - \hat{x}_{i,t,\text{saccade}} \right\|^2}{\sum_k (\tilde{x}_{i,t} - \langle \tilde{x}_{i,t} \rangle_k)^2}$$

where

$$\hat{x}_{i,t,\text{saccade}}(k) = \beta_{0,i,t} + \beta_{\text{choice},i,t}\text{choice}(k)$$

Separability of decoding matrices

To describe whether population encoding of saccade-direction is static or dynamic on single trials, we analyzed single-trial decoding matrices. In analogy to the cross-temporal decoding analyses from Figure 3b, we decouple training and testing time: vertical axis determines the times the decoders were defined and the horizontal axis the times they were tested. Importantly, we now analyze the decoding matrix of each trial separately, whereby each entry is the decoding error, i.e. the unsigned angular difference between the decoder's output and the true saccade direction, which can take values between 0 and 180 degrees. The average decoding matrix was computed using the decoding accuracy, which can be only 0 or 1.

Note that the single-trial decoding matrices are computed using a fixed set of time-dependent decoders, which are optimized to minimize the misclassification rate of saccade direction *on average* (same decoders from Figure 3b). We know that these decoders are different from each other, due to the dynamic signature of the averaged decoding matrix (Figure 3b).

We first de-noised the single-trial decoding matrices by projecting the data onto the first 50-100 principal components to preserve 50% of variance. The dimensionality of the data is $L \times T^2$ where L represents the total number of trials across 9 sessions and T^2 is the dimensionality of each single-trial decoding matrix *training times* × *testing times* (T = 60 over-lapping bins of length 100ms between 0.1 and 0.7s post-saccade).

To describe whether population encoding on single trials is static or dynamic, we ask whether the respective decoding matrix is "separable", meaning that it can be described as the outer product of two vectors (Suppl. Fig 8a; similar to how space-time separability in receptive fields can be measured[8]). A stationary pattern of activity requires only one decoder for classification. The decoder's output (and error) is described by a temporal profile plus a baseline. The temporal profile of the decoder's error does not depend on the decoder, but on the potential pattern's strength modulation - stronger signal leads to lower errors and vice-versa. The baseline depends on the decoder - 0 degrees for optimal ('correct') decoders and an arbitrary value for 'wrong' decoders.

Static encoding can, thus, be well separated into a product of two temporal profiles v_1 and u_1 (Suppl. Fig. 8b), where v_1 (horizontal axis) describes how the strength of saccade-related activity varies throughout the trial, i.e. the temporal profile, and u_1 (vertical axis) describes which of the trained decoders works best for the trial, i.e. the baseline.

In contrast, the decoding matrix of a non-stationary pattern requires different decoders at different time and cannot be well separated in this fashion.

We computed the separable approximation to each single-trial decoding matrix. This is the rank-1 approximation, using the first pair of singular vectors.

$$A^{pca50} = USV^T$$

$$A^{pca50}_{separable} = s_1 u_1 v_1^T$$

Error of separability is defined as the reconstruction error between the original de-noised decoding matrix and its separable approximation:

$$error_{separability} = \sqrt{\frac{1}{T^2}\sum_i^T \sum_j^T \left(a_{ij}^{pca50} - a_{separable,ij}^{pca50}\right)^2}$$

where low errors correspond to static encoding (separable matrices) and high errors correspond to dynamic encoding (non-separable matrices).

We compared the distribution of errors-of-separability obtained from the neural data to the one obtained from simulated responses. The simulated rates matched the mean of condition-averaged responses with trial-by-trial variability was drawn from a Poisson distribution. In the simulation, the distribution of error-of-separability values is very narrow – all single-trials closely resemble the average decoding matrix. This finding promotes the idea that the dynamic encoding of saccade direction is not solely a consequence of the saccade-locked and averaged unit properties.

Method validation

Decoding matrices

Grouping together single-trial decoding matrices based on their error-of-separability resulted in five averaged decoding matrices that look progressively more dynamic (Figure 7c, upper row).

Correlation matrices

Interestingly, we retrieved the same transition from stable to dynamic encoding also from population responses (Figure 7c, lower row). We obtain reconstructed, de-noised population responses by projecting the population responses into the subspace with the most variance in the condition averages. This subspace can thus contain variance due to saccade-direction and time. From these de-noised population responses we computed cross-temporal correlation matrices, whereby each entry quantifies the linear correlation between population responses from different times in the trial. Sorting these single-trial correlation matrices according to the error of separability computed from the decoding matrices revealed the same gradual decrease of values off-diagonal that capture 'block'-like and 'diagonal'-like structures.

The direct, one-to-one mapping between binned decoding matrices and binned correlation matrices need not be the case. In principle, we could have a single pattern of activity that is modulated by task-condition (i.e. saccade-direction), but several patterns that are modulated independently from task-condition (i.e. condition-independent time-related). In this example, we expect a *stable decoding matrix* of saccade-direction, even though the population code is dynamic, thus resulting in a *dynamic correlation matrix*. The fact that the separability-binned correlation matrices also progressively become more dynamic implies that in our data there is not such a drastic difference between condition-dependent and condition-independent modulations, i.e. population code is more stable on trials with stable decoding matrices than on trials with dynamic decoding matrices. Condition-independent modulations are, nonetheless, present, as quantified by the strong diagonal structure in the binned correlation matrix computed on trials close to 0 error of separability.

References

1. Evarts, E. V. Pyramidal tract activity associated with a conditioned hand movement in the monkey. *J. Neurophysiol.* **29**, 1011–1027 (1966).

2. Judge, S. J., Richmond, B. J. & Chu, F. C. Implantation of magnetic search coils for measurement of eye position: an improved method. *Vision Res.* **20**, 535–538 (1980).

3. Suner, S., Fellows, M. R., Vargas-Irwin, C., Nakata, G. K. & Donoghue, J. P. Reliability of Signals From a Chronically Implanted, Silicon-Based Electrode Array in Non-Human Primate Primary Motor Cortex. *IEEE Trans. Neural Syst. Rehabil. Eng.* **13**, 524–541 (2005).

4. Santhanam, G., Ryu, S. I., Yu, B. M., Afshar, A. & Shenoy, K. V. A high-performance brain–computer interface. *Nature* **442**, 195–198 (2006).

5. Mould, M. S., Foster, D. H., Amano, K. & Oakley, J. P. A simple nonparametric method for classifying eye fixations. *Vision Res.* **57**, 18–25 (2012).

6. Bruce, C. J. & Goldberg, M. E. Primate frontal eye fields. I. Single neurons discharging before saccades. *J. Neurophysiol.* **53**, 603–35 (1985).

7. A Graf, A. B., Kohn, A., Jazayeri, M. & Anthony Movshon, J. Decoding the activity of neuronal populations in macaque primary visual cortex. *Nat. Neurosci.* **14**, (2011).

8. DeAngelis, G. C., Ohzawa, I. & Freeman, R. D. Receptive-field dynamics in the central visual pathways. *Trends Neurosci.* **18**, 451–458 (1995).